A Toolbox of IgG Subclass-Switched Recombinant Monoclonal Antibodies for Enhanced Multiplex Immunolabeling of Brain

Nicolas P. Andrews[1], Justin X. Boeckman[1], Colleen F. Manning[1], Joe T. Nguyen[2], Hannah Bechtold[2], Camelia Dumitras[1], Belvin Gong[1], Kimberly Nguyen[1], Deborah van der List[1], Karl D. Murray[1], JoAnne Engebrecht[3], and James S. Trimmer[1,3]

Departments of [1]Neurobiology, Physiology and Behavior, [2]Molecular and Cellular Biology, and [3]Physiology and Membrane Biology, University of California, Davis, CA 95616

Address correspondence to James S. Trimmer, PhD, Department of Neurobiology, Physiology and Behavior, University of California, One Shields Avenue, Davis, CA 95616-5270. E-mail: jtrimmer@ucdavis.edu

Acknowledgments

This work was funded by NIH research grants U24 NS050606, R24 NS092991 and U24 NS109113 to J. S. Trimmer. We thank the current and former staff members of the UC Davis/NIH NeuroMab Facility and the Trimmer laboratory for their contributions and dedicated efforts, and Dr. Randall Stewart at the National Institute of Neurological Disorders and Stroke for support and helpful advice. We thank Dr. Gavin Wright of the Sanger Institute for his generous gift of the P1316 expression plasmid and helpful advice.

Abstract

Generating recombinant monoclonal antibodies (R-mAbs) from mAb-producing hybridomas offers numerous advantages that increase the effectiveness, reproducibility, and transparent reporting of research. We report here the generation of a novel resource in the form of a library of recombinant R-mAbs validated for neuroscience research. We cloned immunoglobulin G (IgG) variable domains from cryopreserved hybridoma cells and input them into an integrated pipeline for expression and validation of functional R-mAbs. To improve efficiency over standard protocols, we eliminated aberrant Sp2/0-Ag14 hybridoma-derived variable light transcripts using restriction enzyme treatment. Further, we engineered a plasmid backbone that allows for switching of the IgG subclasses without altering target binding specificity to generate R-mAbs useful in simultaneous multiplex labeling experiments not previously possible. The method was also employed to rescue IgG variable sequences and generate functional R-mAbs from a non-viable cryopreserved hybridoma. All R-mAb sequences and plasmids will be archived and disseminated from open source suppliers.

Introduction

Antibodies (Abs) are the workhorses of biomedical research. Enhancing the research community's access to extensively validated Abs remains an important goal of antibody developers in both academia and industry (1). This has been the topic of a number of recent conferences and commentaries, led to changes in journal practices as related to transparent reporting of antibody-based research including the use of RRIDs, and resulted in large-scale NIH and EU Ab development initiatives (*e.g.*, the NIH Common Fund Protein Capture Reagent Program, the EU Affinomics Program). It is widely recognized that production of Abs in a renewable form, such as monoclonal antibodies (mAbs), represents a substantial advance over polyclonal Abs from antisera that are available in finite quantity, and that comprise a heterogeneous and less definable population of Abs (2-4). Having mAbs available in recombinant form as recombinant mAbs (R-mAbs) offers numerous additional advantages (5). Recombinant expression systems allow for the reliable production of an R-mAb not prone to loss by genetic instability of tetra- or hexa-ploid hybridoma cells or other factors (6, 7). Moreover, unlike hybridoma cell lines that can express multiple functional heavy and light immunoglobulin chains (8-10), recombinant expression ensures production of a single, molecularly defined R-mAb. Recombinant expression can also yield production levels 100s or 1000s of times higher than is possible with endogenous expressions of mAbs from hybridoma cells [*e.g.*, (11-13), etc.]. Furthermore, the cloning of R-mAbs provides for permanent, dependable and inexpensive archiving of the R-mAb as plasmid DNA and nucleic acid sequences versus an archiving system relying on expensive cryopreservation of hybridoma cell lines in liquid nitrogen, and their subsequent recovery as viable cell cultures. The conversion of existing mAbs to R-mAbs also allows for more effective dissemination of R-mAbs as plasmids, bacterial stocks or as DNA sequences. However, in spite of these advantages, it remains that most mAbs used for research are produced by hybridomas in culture.

Modern techniques employing Abs as immunolabels [*e.g.*, immunoblotting (IB), immunocytochemistry (ICC) and immunohistochemistry (IHC)] utilize simultaneous multiplexing of numerous Abs to simultaneously detect multiple targets within a single cell or tissue sample. This allows for direct comparison of the relative amounts and respective characteristics of multiple target molecules within the same sample, while reducing the number of samples needed to accomplish a comprehensive analysis. Typically, the individual primary Abs bound to the sample are detected with secondary antibodies conjugated to distinct reporters, most commonly organic fluorescent dyes, although enzymes, gold particles, etc. are also routinely employed as detection modalities. Multiplex labeling is often accomplished using Abs raised in distinct species, with their subsequent individual detection accomplished using species-specific secondary antibodies. However, mouse mAbs offer an important advantage for multiplex labeling procedures. Each mouse mAb is a single immunoglobulin (Ig) isotype, generally of the IgG class and if so specifically of a single IgG subclass, most commonly IgG1, IgG2a or IgG2b. Mouse mAbs of distinct IgG subclasses can be robustly, reliably and specifically detected with commercial subclass-specific secondary antibodies, and, as such, can be multiplexed in a manner analogous to Abs from different species [*e.g.*, (14-18)]. One limitation to greater adoption of this approach is that mouse mAb collections generally have an extremely high representation (≈70%) of IgG1 mAbs (18), which limits the flexibility of multiplex labeling. The conversion of mAbs into R-mAbs allows for their subsequent engineering into forms with properties distinct from their parent mAb, as is routinely done to impact diverse aspects, including target binding affinity, of therapeutic R-mAbs (19). Such engineering could also include switching the heavy chain constant region to impact subclass-specific secondary Ab binding specificity, an approach similar to that used to successfully modify subclass-specific *in vivo* effector functions (20).

There are numerous routes to obtaining validated R-mAbs, including their *de novo* generation from high complexity immune repertoire libraries produced from naïve or immunized animals, combined with selection of target-specific R-mAbs by *in vitro* display (21). Alternatively,

R-mAbs can be generated from existing hybridoma cell lines, which express well-characterized mAbs [*e.g.*, (22)]. Here we undertook conversion of a widely used collection of hybridoma-generated mAbs extensively validated for neuroscience research applications (14, 23, 24) into recombinant form. We developed a coherent pipeline of protocols for effective cloning of intact R-mAbs from cryopreserved hybridoma cells and their subsequent validation compared to their parent mAbs. Further, we developed a process to engineer these R-mAbs to IgG subclass-switched forms that provide additional utility for multiplex labeling employing mouse IgG subclass-specific secondary Abs. This approach is feasible and relatively inexpensive for any laboratory that uses standard molecular biology and mammalian cell culture techniques. This approach also represents a reliable method to convert valuable cryopreserved hybridoma collections to the immortalized form of a DNA sequence archive, including hybridomas that are no longer viable in cell culture.

Results

Effective Cloning of Immunoglobulin V_H and V_L Regions from Cryopreserved Hybridomas and Generation of R-mAbs

We previously generated a large library of mouse mAbs that have been extensively validated for efficacy and specificity for immunolabeling endogenous target proteins in mammalian brain samples in immunoblotting (IB) and immunohistochemistry (IHC) applications (14, 23, 24). Here, we undertook the systematic conversion of a sizable subset of this existing mAb collection to R-mAbs. We developed an innovative pipeline for R-mAb cloning, expression and validation. For the cloning steps, we built upon a previously described method (22, 25) to clone IgG V_H and V_L region sequences, but with the modification that we cloned directly from cryopreserved hybridomas, without the need for their labor-intensive recovery into cell culture. Our overall cloning strategy (Figure 1A) employs PCR-mediated amplification to generate IgG V_H and V_L region sequences from hybridoma-derived cDNA, followed by PCR-based fusion of these V_H and

V_L regions with a joining fragment that contains a subset of the elements needed for high level expression of R-mAbs from transfected mammalian cell lines. The product of this fusion PCR reaction is then inserted into a plasmid containing the remainder of the elements for propagation in bacteria and expression of intact heavy and light chains in, and secretion of R-mAbs from, transfected mammalian cells (Figure 1B).

We extracted RNA from cryopreserved hybridoma cell vials, followed by first strand cDNA synthesis and RT-PCR of the IgG V_H and V_L region sequences (Figure 1A). To enhance throughput, we performed the first three steps of this process in a 96 well plate format. We obtained hybridoma cells directly from cryovials and added an aliquot of 1-3 x 10^6 cells to individual wells of a commercially available 96 well RNA extraction plate. After performing the RNA isolation procedure in the 96 well plate, we replica plated 1/16 of the extract volume to a second 96 well plate for first strand cDNA synthesis. Following the cDNA synthesis reaction, we replica plated ≈5% of the volume of the cDNA synthesis product to a third 96 well plate to serve as the template for PCR amplification of the IgG V_H and V_L domain sequences. As such, the templates for the V_H and V_L domain PCR amplification represented the cDNA yield from ≈3,000-7,500 hybridoma cells. We amplified the IgG V_L kappa (κ) and V_H domain sequences from the hybridoma cDNA templates using a degenerate mouse Ig variable region primer set developed by Gavin Wright and colleagues (22) expanding on a previously used set (33) that at the time of their design recognized 97% and 98% of known functional heavy and kappa (κ) light chain sequences, respectively. Lambda light chains were not targeted for amplification because they constitute only a small percentage of light chains used in mouse immunoglobulins (34, 35). This PCR amplification reliably gave products of the expected 360 base pairs (bp) for both the V_L and V_H domain sequences, examples of which are shown in Figure 2A for representative mAbs N59/36 (“N59”, anti-NR2B/GRIN2B glutamate receptor) and K39/25 (“K39”, anti-Kv2.1/KCNB1 potassium channel).

To permit cloning of both the V_H and V_L regions into a single expression vector, fusion PCR (F-PCR) was performed using as templates the V_H and V_L PCR products, as well as a joining fragment amplified from the P1316 expression plasmid (22, 25) to produce a 2.4 kbp amplicon (Figure 2B). The joining fragment (Figure 1B) contains kappa light chain constant region sequences and an associated polyadenylation signal, followed by a CMV promoter to drive V_H expression, and a V_H leader sequence (22, 25). The F-PCR reaction products were then treated with NotI and AscI restriction enzymes and purified in preparation for cloning into a NotI/AscI restriction enzyme-digested fragment of the P1316 expression plasmid (Figure 1B). Upstream of the NotI cloning site, the digested P1316 fragment contains a CMV promoter to drive light chain expression and a V_L leader sequence, and downstream of the AscI cloning site a mouse IgG1 C_H sequence, and a polyadenylation signal (Figure 1B). Standard methods were used for DNA ligation and subsequent transformation of *E. coli*. Clones expressing the full-length IgG expression cassette were identified by colony PCR (Figure 2C). Following NotI/AscI restriction digestion to verify the correct insert size (Figure 2D), these plasmid clones were subjected to further analysis (Figure 1A), including expression in mammalian cells, and R-mAb validation and sequencing as detailed in the subsequent sections.

While a number of *bona fide* R-mAbs were isolated using this approach, we found a high degree of variability in the number of colony PCR- and restriction enzyme digest- verified positive plasmids that yielded functional expression. A major obstacle in cloning functionally rearranged IgG sequences from many mouse hybridomas is the presence of an aberrant kappa IgG light chain transcript expressed by the Sp2/0-Ag14 (Sp2/0) hybridoma (36) that frequently serves as a "myeloma" partner for fusion with mouse splenocytes to generate mAb-producing hybridomas (37) , and that was used as the fusion partner in all of our mAb generation efforts (14, 24). The source of this non-productive IgG light chain is the MOPC-21 myeloma cell line used to generate the Sp2/0 hybridoma (37). As we experienced, and as previously reported by others (36), aberrant chain mRNA expression varies greatly among distinct hybridoma cell lines but in certain cases

166 can exceed the levels of functional light chain transcripts. For certain of our projects, this resulted
167 in >90% of the colony PCR positive clones failing to produce detectable levels of functional R-
168 mAbs, thus necessitating a high volume of screening.

169 As such, we sought to eliminate this aberrant light chain during the cloning process. We
170 treated the V_L PCR products with the restriction enzyme BciVI, as the restriction site for this
171 enzyme is present in the V_L region of the aberrant Sp2/0-derived transcript, but is predicted to
172 occur at a low frequency in functional mouse V_L kappa sequences (38). We used V_L PCR products
173 derived from the Sp2/0 cell line and from pooled BALB/c mouse splenocytes as positive and
174 negative controls, respectively, for sensitivity to BciVI digestion. Due to the exclusive presence of
175 aberrant light chain in Sp2/0 cells, V_L PCR products from these cells were completely digested,
176 as shown by the decreased size of the V_L PCR products from ≈360 bp typical of V_L PCR products
177 (see Figure 2A for examples) to the ≈180 bp fragment that results from BciVI digestion (Figure
178 2E). In contrast, the sample prepared from the pooled mouse splenocytes was not detectably
179 affected by BciVI digestion (Figure 2E). Treatment of V_L PCR products from various Sp2/0-derived
180 hybridomas with BciVI resulted in varying degrees of digestion, yielding different proportions of
181 the bands representing the intact V_L PCR product of ≈360 bp and the cleaved aberrant SP2/0-
182 derived V_L fragment of ≈180 bp (Figure 2E). After BciVI digestion was incorporated into the
183 protocol, DNA sequencing of 149 colony PCR-positive clones from 26 different hybridomas
184 revealed that only 12 (8%) still contained the aberrant V_k light chain (Table 1). In certain cases,
185 digestion of hybridoma V_L PCR products resulted in fragments of unexpected sizes (see the
186 K58/35 lane in Figure 2E), indicating, as predicted by an earlier bioinformatics analysis (38), that
187 in rare cases (in our hands, 3/248 clones pursued to this step) the BciVI restriction site was also
188 present in these functionally rearranged splenocyte-derived V_L genes. As such, we attempted to
189 clone these V_L PCR products without BciVI treatment. As one example, the splenocyte-derived V_k
190 light chain PCR products from the K58/35 hybridoma were sensitive to BciVI digestion, which
191 necessitated their cloning in the absence of the BciVI digestion step. This project yielded

somewhat lower frequency of clones that produced functional R-mAbs able to detect target antigen (≈37%) than, on average, those containing splenocyte-derived V_L PCR products refractory to BciVI digestion (≈48%; Table 2). For the bulk of mAbs encoded by splenocyte-derived V_L PCR products resistant to BciVI digestion, ligations were performed following BciVI digestion, and 10-14 candidate clones that were colony PCR-positive were selected. Plasmid DNA was digested with AscI/NotI restriction enzymes to confirm the correct insert (Figure 2D). On average, ≈93% of all clones subjected to restriction analysis passed this screening step.

We next transfected the colony PCR and restriction digest-validated plasmids into COS-1 cells cultured in 12 well or 96 well tissue culture plates. After a 3 to 6 day incubation, we tested the conditioned culture media for production of target-specific R-mAbs. While the parent mAbs had previously been validated for efficacy and specificity in a variety of applications (IF-ICC, IB and IHC on brain samples), we selected the IF-ICC assay in transiently transfected heterologous cells for R-mAb validation. This method was chosen because it is high-throughput, employing 96 well microtiter plates, it requires only a small amount of R-mAb sample, and the robust difference between target-expressing and non-expressing cells in the same sample allows for sensitivity and clarity of results. Importantly, each of the parent mAbs had been previously validated in this procedure. We took advantage of the fact that in most cases we switched the IgG subclass during conversion of the hybridoma-derived mAb into the corresponding R-mAb, allowing for their separate detection by subclass-specific secondary Abs (18). This assay involved expressing the full-length target protein in transiently transfected COS-1 cells cultured in individual wells of a black polystyrene 96 well clear bottom plate that allows for microscopic visual analysis and imaging using indirect immunofluorescence. For each of 1 to 15 R-mAb candidate clones to be assayed from a given project, a set of replicate wells were prepared expressing the given target protein. After fixation and permeabilization, the individual wells were then immunolabeled with either the hybridoma-generated mAb alone, the R-mAb alone, or the mAb and R-mAb together. Each well was subsequently incubated with a cocktail of the two distinct subclass-specific

secondary Abs, one specific for the respective mAb and one specific for the subclass-switched R-mAb mouse IgG subclasses, and both conjugated to spectrally distinct Alexa Fluors. The "mAb only" well was used to demonstrate that the target protein was expressed in a subset of the transiently transfected cells, and that the only detectable secondary Ab labeling was for the IgG subclass of the parent hybridoma-generated mAb. Similarly, the R-mAb only wells were used to show that the R-mAb labeled a comparable number of cells, and that the only detectable secondary Ab labeling was for the IgG subclass of the subclass-switched R-mAb. The wells containing both the parent mAb and candidate R-mAb were used to show that the mAb and R-mAb gave indistinguishable labeling patterns at both the cellular and subcellular level and could be detected separately using subclass-specific secondary Abs. Numerous examples of this assay are shown in the following sections focusing on specific R-mAb projects. We note that only in rare cases was the labeling for one or both secondaries noticeably depressed in the well containing both mAb and R-mAb relative to the wells with these primary antibodies alone, as would occur due to competitive binding to the same epitope. However, this was generally not apparent, suggesting that in this assay system, in which the target protein was overexpressed, we were typically operating under conditions of antigen excess.

In comparing the overall results from 180 recent projects that had BciVI-resistant splenocyte-derived V_L PCR products, and that were taken through this entire pipeline one time (Table 2), we found that a range of 1-15 colony PCR- and restriction digest-positive candidate R-mAbs per project were evaluated in the COS-ICC assay (919 total, mean/project = 5.11 ± 0.23 S.E.M.). For these 180 projects, cloning was performed after BciVI digestion, and all restriction digest-validated candidates were tested for functional mAb production. Of these 180 projects, 72% (129 projects) yielded at least one positive R-mAb on their first pass through the pipeline. A retrospective analysis of these 129 successful projects revealed a range of 1 to 13 restriction digest-validated candidates were evaluated (mean/project = 5.74 ± 0.26 S.E.M.), with an overall success rate of 48.4% for all 741 restriction digest-validated candidate R-mAbs tested. A parallel

244 analysis of the 51 projects that did not yield a positive R-mAb on their first pass through the
245 pipeline revealed a similar range of 1 to 15 restriction digest-validated candidates per project
246 evaluated. However, an overall lower number of colony PCR- and restriction digest-positive
247 candidates were evaluated in the COS-ICC assay (178 total, mean/project = 3.5 ± 0.37 S.E.M.)
248 in these projects than for the successful projects. A statistically significant difference (two-tailed
249 P value = 2.48×10^{-6}) existed between the number of candidates evaluated in successful versus
250 unsuccessful projects. The per-project COS-ICC rate success was impacted by number of clones
251 tested. For 1-3 clones tested (66 projects), the project success rate was 50%, for 4-6 (62 projects)
252 it was ≈ 77%, and for ≥ 7 (52 projects) it was ≈92%. However, the per clone success rate was
253 similar between the three bins (≈ 45% vs. ≈39% vs. ≈ 45%).

254 Following validation in the COS-ICC assay, a subset of positive clones for each project
255 was subjected to DNA sequencing. We employed a set of sequencing primers that allowed for
256 determination of sense and antisense strands of the V_H and V_L domain-encoding cDNA inserts
257 that were unique to each R-mAb. The sequences were searched against the NCBI database, and
258 against a custom database that contained the V_H and V_L domain sequences of the parent P1316
259 plasmid, the V_L domain of the aberrant Sp2/0 cell line, and the V_H and V_L domain sequences of
260 all of the R-mAbs we had cloned to date. The set of COS-ICC validated R-mAb plasmids derived
261 from a single hybridoma that had matching sequences unique from any sequences in the custom
262 database were subsequently archived as frozen plasmid DNA and bacterial glycerol stocks, and
263 their sequence used as the archival sequence of that particular R-mAb.

264

265 **Effective Cloning and IgG Subclass Switching of a Widely Used Monoclonal Antibody**

266 We initiated our R-mAb cloning efforts with the K28/43 mAb, a mouse mAb specific for the neural
267 scaffolding protein PSD-95. This mAb is widely used as a marker of excitatory synapses (*e.g.*, as
268 of 7/1/18 ≈500 publications have cited the use of the K28/43 mAb as obtained from the UC
269 Davis/NIH NeuroMab Facility alone). While the K28/43 mAb is already of a less common IgG

subclass (IgG2a), generating a subclass switched version with an alternate IgG subclass would provide greater flexibility in its use in multiplex labeling experiments, and also provide proof of concept that we could use our process to effectively generate subclass switched R-mAbs with efficacy and specificity comparable to the parent mAb. We generated V_L and V_H domain cDNA fragments from the cryopreserved K28/43 hybridoma and cloned them into the original P1316 plasmid that contains a mouse IgG1 C_H domain (22). COS-1 cells were transiently transfected with the resultant plasmids. We evaluated the conditioned medium from the transfected cells for the presence of the subclass-switched K28/43R IgG1 R-mAb by ICC against fixed and permeabilized transiently transfected COS-1 cells expressing full-length PSD-95 (Figure 3A). We note that we have designated the recombinant R-mAb versions of each of our mAbs by a capital "R" after the clone designation, in this case the R-mAb cloned from the K28/43 hybridoma is designated K28/43R. We screened the COS-1 cell-generated R-mAbs for functional R-mAb immunoreactivity in the 96-well IF-ICC assay detailed in the previous section. After primary antibody labeling, all wells received both IgG1- and IgG2a-subclass-specific, fluorescently labeled secondary antibodies. As shown in Figure 3A, as expected, the sample receiving only the native K28/43 hybridoma-generated mAb exhibited a signal corresponding to the IgG2a subclass-specific secondary Ab (red) with no detectable signal for the IgG1 subclass-specific secondary Ab (green). Conversely, labeling with the K28/43R R-mAb alone produced only an IgG1 subclass-specific green signal demonstrating a successful IgG subclass switch for the R-mAb (Figure 3A). Simultaneous multiplex labeling with the hybridoma-generated mAb and a positive R-mAb resulted in an identical pattern of immunolabeling at the cellular level in the specific cells recognized, and at the subcellular level as to the pattern of immunolabeling within the labeled cells, as shown by the uniform hue of the signal in the merged panel, indicating that both the mAb and R-mAb were recognizing the same target (Figure 3A). We next performed multiplex immunofluorescent IHC on adult mouse brain sections with the K28/43 mAb and the K28/43R R-mAb. As shown in Figure 3B, as detected with secondary Abs specific for their respective mouse

IgG subclasses, the signal from these two primary antibodies was indistinguishable in its laminar and subcellular pattern in cerebellar cortex, consistent with previous studies of PSD-95 [*e.g.*, (39)]. Both signals were especially intense in the terminal pinceau of basket cells located adjacent to the Purkinje cell layer, and both signals were also present in the molecular layer, and for the most part lacking in the granule cell layer (Figure 3B). This demonstrates that consistent with the validation in heterologous COS-1 cells expressing exogenous PSD-95, the K28/43 R-mAb can be used reliably for multiplex immunolabeling of endogenous PSD-95 in brain sections.

The specificity of recombinant K28/43R was also assessed on immunoblots of samples from COS-1 cells exogenously expressing various representatives of the MAGUK superfamily of scaffolding proteins, of which PSD-95 is one member (Figure 3C-D). Immunoblots were probed with a rabbit polyclonal antibody raised against PSD-95 and that also cross-reacts with SAP97 as a positive control, and recombinant K28/43R in either the IgG1 or IgG2a mouse IgG subclass form (Figure 3C-D). Generation of the IgG2a expression plasmid is described below. Both the IgG1 and IgG2a subclass isoforms of the K28/43R R-mAb gave identical immunolabeling patterns against samples from rat brain and COS-1 cells overexpressing PSD-95. Moreover, the pattern of R-mAb immunolabeling was similar to that obtained with the rabbit polyclonal antibody, and absent against samples of COS-1 cells exogenously expressing other MAGUK superfamily members (Figure 3C-D). To confirm expression of these MAGUK proteins, immunoblots were probed with rabbit polyclonal anti-PSD-95 and with the hybridoma-generated K28/43 mAb (IgG2a) or a mAb that recognizes all mammalian MAGUK proteins mAb (K28/86; IgG1) (27) (Figure 3E). These initial results demonstrated that we could use this cloning and expression process to generate and validate subclass-switched R-mAbs that recapitulate the immunolabeling characteristics of the native mAbs.

Generation of an R-mAb Expression Plasmid with an IgG2a C_H Backbone Allows for Effective Subclass Switching of mAbs from Prevalent IgG1 Subclass

Most (≈70%) mouse IgG mAbs are of the IgG1 subclass (18). Generating R-mAbs employing the efficient V_H and V_L cloning approach developed by Gavin Wright and colleagues includes their subsequent insertion into an expression plasmid that yields R-mAbs of the mouse IgG1 subclass due to the presence of the mouse γ1 C_H domain in the plasmid backbone (22). To generate R-mAbs of less common mouse IgG subclasses, we set out to modify this plasmid by replacing this γ1 C_H domain with a mouse γ2a C_H domain. We developed PCR primers to amplify the γ2a C_H domain sequence from cDNA generated from the hybridomas producing the K28/43 IgG2a mAb. We then replaced the γ1 C_H domain present in the K28/43R plasmid with this γ2a C_H domain using restriction digestion, gel isolation and ligation. This plasmid was sequenced verified and validated for expression of a K28/43R R-mAb of the IgG2a subclass (Figure 3C).

We subsequently used this plasmid as the target cloning vector for generation and expression of numerous R-mAb plasmids encoding functional IgG2a R-mAbs. Our strategy entailed cloning all native IgG1 and IgG2b mAbs into this plasmid to generate forms distinct from the parent native mAbs. Toward this end, we have successfully cloned and validated as functional R-mAbs a total of 178 mAbs (Table 3). This includes 148 mAbs of distinct subclasses converted to IgG2a R-mAbs (125 IgG1, 21 IgG2b, and 3 IgG3), and 29 IgG2a mAbs that were retained in their native IgG subclass (Table 3). We also converted the IgG2a mAb K28/43 to an IgG1 R-mAb. Each of these R-mAbs have been assigned unique RRID numbers in the Antibody Registry (Table 3) and all will be deposited in plasmid form at Addgene, a subset of which are already available (https://www.addgene.org/James_Trimmer/).

Multiplex brain immunofluorescent labeling with subclass switched R-mAbs

One benefit of subclass switching R-mAbs is the ability to perform multiplex immunolabeling previously not possible due to subclass conflicts. Examples of such enrichment in cellular protein localization are shown in Figure 4. Figure 4A shows labeling with the subclass switched IgG2a R-mAb derived from the widely used pan-voltage-gated sodium channel or "pan-Nav channel" IgG1 mAb K58/35 (40). Like the corresponding mAb, K58/35 R-mAb gives robust labeling of Nav channels concentrated on the axon initial segment (AIS, arrows in Figure 4A main panel), and at nodes of Ranvier (arrows in Figure 4A insets). Importantly, subclass switching allowed Nav channel labeling at nodes to be verified by co-labeling with K65/35 an IgG1 subclass antibody directed against CASPR, a protein concentrated at paranodes (41, 42). Similarly, simultaneous labeling for the highly-related GABA-A receptor β1 and β3 subunits (43) with their widely used respective mAbs N96/55 and N87/25 could not be performed as both are IgG1 subclass. Switching N96/55 to IgG2a allowed simultaneous detection of these two highly-related but distinct GABA-A receptor subunits. In Figure 4B localization of GABA-A receptor β1 and β3 subunits appeared completely non-overlapping in separate layers of cerebellum. Figure 4C illustrates localization of protein Kv2.1 and AnkyrinG in separate subcellular neuronal compartments. Labeling for the K89/34R R-mAb (IgG2a, red), specific for the Kv2.1 channel, highly expressed in the plasma membrane of the cell body and proximal dendrites (arrows in panel C1) is shown together with labeling for N106/65 (green), an IgG1 mAb specific for AnkyrinG, a scaffolding protein highly expressed in the AIS (arrows in panel C2) and at nodes of Ranvier. Subclass switching N229A/32 (IgG1, GABA-AR α6) to IgG2a, allows comparison with Kv4.2 potassium channel (K57/1, IgG1) in the cerebellum where both are highly expressed in the granule cell layer (Figure 4D). While both are prominently found in the glomerular synapses present on the dendrites of these cells, simultaneous labeling reveals that some cells express both (Figure 4D, magenta) while others appear to predominantly express Kv4.2 (Figure 4D, blue). Labeling for both

proteins is in contrast to that for mAb N147/6 (IgG2b) which recognizes all isoforms of the QKI transcription factor and labels oligodendrocytes within the granule cell layer and throughout the Purkinje cell layer (PCL, green). In Figure 4E, localization of pan-QKI (N147/6, IgG2b, blue) is compared with GFAP (N206A/8, IgG1, green) predominantly thought to be in astrocytes. Surprisingly many (but not all) cells co-label both proteins. We also labeled cortical neurons with these two mAbs (pan-QKI in blue, GFAP in green). Multiplex labeling for the neuron-specific Kv2.1 channel, using subclass-switched K89/34R (IgG2a, red) confirms non-neuronal localization of both proteins. Lastly, we labeled for the postsynaptic scaffold protein PSD-93 using R-mAb N18/30R (IgG2a, red), which in the cerebellum is prominently localized to Purkinje cell somata and dendrites (44). As shown in Figure 4F, the R-mAb labeling is consistent with the established localization of PSD-93. Because of subclass switching the N18/30R R-mAb, this labeling can now be contrasted with labeling for the excitatory presynaptic terminal marker VGluT1, labeled with mAb N28/9 (IgG1, blue), which exhibits robust labeling of parallel fiber synapses in the molecular layer, and glomerular synapses in the granule cell layer. Together these results demonstrate the utility of employing subclass-switched R-mAbs to obtain labeling combinations not possible with native mAbs.

Recovery of Functional R-mAbs from a Non-Viable Hybridoma

While not a common event, mAb-producing B cell hybridomas can lose their mAb production due to genetic instability (45-47), mycoplasma contamination leading to amino acid depletion and cytopathic effects (48), or other factors. Non-optimal cryopreservation due to problems during the freezing process itself or inadequate storage conditions can result in non-recoverable frozen seeds. As the method described here for cloning of V_H and V_L domain sequences from cryopreserved hybridomas does not require expansion of cells in culture prior to RNA extraction, we speculated that it may be possible to use this approach to generate functional R-mAbs from even those hybridoma cell lines that are no longer viable in cell culture.

We had in our cryopreserved hybridoma archive a hybridoma cell line that produced the D3/71 mAb. This hybridoma cell line had been generated in 1994 among a series of projects targeting the Kv2.1 voltage-gated potassium channel α subunit, projects that also yielded the D4/11 mAb (14). The D3/71 mAb has particular value in binding at a site distinct from other anti-Kv2.1 mAbs. In particular, the binding site for the D3/71 mAb, but not most other available anti-Kv2.1 mAbs (and pAbs), remains intact in truncated isoforms of Kv2.1 found in patients with severe neurodevelopmental disorders linked to *de novo* frameshift or nonsense mutations in the KCNB1 gene (49, 50). Unlike our experience with other cryopreserved hybridomas in our collection, when we attempted to resuscitate this cryopreserved hybridoma cell line over 20 years after it was cryopreserved, the D3/71 hybridoma cells were no longer viable in cell culture. We extracted RNA from a cryopreserved vial of D3/71 hybridoma cells in an attempt to generate a functional D3/71R R-mAb from these non-viable hybridoma cells. Cloning was performed as described above including insertion of D3/71 V_H and V_L domain cDNA into the mouse IgG2a expression plasmid (Figs. 5A-B). After bacterial transformation, most of the colonies tested (20/24) were positive for the insert by PCR (Figure 5C). Restriction analysis of 12 PCR positive clones confirmed that they each contained the full-length V_L-joining fragment-V_H cassette (Figure 5D). We next tested whether these plasmids encoded functional D3/71R R-mAb in double immunolabeling experiments in Kv2.1-expressing transiently transfected COS-1 cells using a distinct native anti-Kv2.1 IgG1 mAb K89/34 (51) as a control. We also included a comparison of D3/71R to the subclass-switched K89/34R R-mAb (31, 52) as an additional control. Two out of 12 clones exhibited specific immunolabeling of Kv2.1-expressing cells as detected with an anti-IgG2a secondary antibody. An example for one of these is shown in Figure 6A. As shown for one of the positive clones, the recovered D3/71R R-mAbs exhibited immunolabeling that when detected with an IgG2a-specific secondary antibody (red) was indistinguishable at both the cellular level in the specific cells recognized, and at the subcellular level as to the pattern of immunolabeling within the labeled cells, to that obtained with the K89/34 IgG1 mAb detected with an IgG1-specific

secondary antibody (green). Parallel experiments demonstrated successful subclass-switching of the K89/34 IgG1 mAb when converted into the K89/34R R-mAb (Figure 6B). Moreover, the D3/71R R-mAb exhibits immunolabeling of endogenous Kv2.1 in neurons in mouse neocortex that recapitulates the previously established pattern of Kv2.1 immunolabeling in these neurons [*e.g.*, (31, 53, 54)] and that overlaps precisely with simultaneous immunolabeling obtained with the native K89/34 mAb (Figure 6C). The D3/71R R-mAb also yields an immunoreactive band on immunoblots similar to that obtained with K89/34 and K89/34R (Figure 6D). These results suggest that the mAb cloning approach described here can be used to effectively recover functional R-mAbs from non-viable hybridomas and could be applied by researchers that have such hybridomas in their collections.

Discussion

In this study, we developed a novel R-mAb generation and validation procedure that we used to generate a valuable R-mAb resource by converting a library of widely used mouse mAbs into recombinant reagents. Our approach was adapted from that of Gavin Wright and colleagues (22) with modifications to facilitate higher throughput cloning and validation steps. The efficiency of the process was further enhanced by restriction digest of V_L PCR products to eliminate the MOPC-21 derived aberrant light chain. R-mAbs were produced in the culture medium from transiently transfected cells under standard mammalian cell culture conditions in sufficient quantities that they did not require purification for effective use in IB, ICC, and IHC assays. We were also able to recover functional R-mAbs from a cryopreserved hybridoma cell line that was no longer viable in cell culture *via* RNA extraction, cloning and expression. Moreover, in the process we generated subclass-switched R-mAbs that are more amenable to multiplex labeling in IB, ICC, and IHC applications. We then employed these mAbs in multiplex IHC experiments in combinations that were not possible prior to their cloning and expression as subclass-switched R-mAbs. Using the method described here, most researchers with standard molecular biology expertise can generate

449 functional R-mAb expression plasmids with the advantages associated with recombinant
450 reagents from their own cryopreserved hybridomas, whether viable or non-viable. Moreover,
451 producing R-mAbs from cells transfected with any of the large collection of expression plasmids
452 whose generation is described here is within the reach of anyone with standard mammalian cell
453 culture capabilities.

454 Building on our long standing and established practice of utilizing mAbs of different IgG
455 subclasses in simultaneous multiplex immunolabeling experiments (14-17), we previously
456 undertook a systematic analysis of anti-mouse IgG subclass-specific secondary antibodies. We
457 demonstrated that the use of mouse mAbs of different IgG subclasses in combination with anti-
458 mouse IgG subclass-specific secondary antibodies for simultaneous multiplex immunolabeling
459 allows for robust and specific labeling in several immunolabeling applications, and also provides
460 enhanced signal-to-noise (background) in immunolabeling of brain samples when compared to
461 generic anti-mouse IgG (H+L) secondary Abs (18). Simultaneous multiplex labeling of multiple
462 targets within a single sample allows for better comparison of their relative levels, co-localization,
463 and overall tissue architecture. Multiplex labeling also conserves valuable samples, as multiple
464 targets can be interrogated in the same sample instead of across multiple samples, which can be
465 a particular concern in studies using human tissue samples that may be available in limited
466 quantity. However, multiplex labeling using the classical approach of employing primary Abs
467 raised in different species and their subsequent detection with species-specific secondary Abs is
468 highly limited by the lack of available Abs from numerous species. As one example, interrogating
469 the Abs registered with the Antibody Registry (2,381,068 as of 9/9/18) shows a preponderance
470 (84% in total) of Abs raised in only three species: rabbits (44.6%), mice (31.2%) and goats (8.2%),
471 with all other species together accounting for the remaining 16%. Among the predominant
472 species, goat Abs are exclusively polyclonal and as such cannot be used with one another in
473 simultaneous multiplex labeling. Moreover, the bulk of secondary Abs are raised in goats,
474 constraining facile detection of primary Abs in multiplex labeling experiments employing goat

primary Abs. Rabbit Abs (whether poly- or mono-clonal) have limited utility for multiplex labeling, as unlike most other mammals, rabbits do not make IgGs of distinct subclasses but only a single generic IgG (55). As such employing multiple goat or rabbit primary Abs for multiplex immunolabeling involves costly and time-consuming procedures such as direct labeling with different fluorophores or sequential multiplexing technologies such as Opal™ (56).

While the utility of mouse mAbs (and less common rat mAbs) for simultaneous multiple immunolabeling is enhanced by the availability of subclass-specific secondary antibodies, it remains that mouse mAbs against any given target may be available in only a single IgG subclass. In general, mouse mAb collections reflect the representation of these subclasses in the circulating serum IgGs in immunized BALB/c mice, which is ≈70% IgG1, ≈20% IgG2a and ≈10% IgG2b (57). As a prominent example, the large mouse mAb catalog of ThermoFisher Scientific (10,992 independent IgG mouse mAbs as of 6/28/18) follows this remarkably closely, comprising 69% IgG1, 18% IgG2a and 12% IgG2b (Matt Baker, ThermoFisher Scientific, personal communication). As such, the flexibility of using mouse mAbs in multiplex labeling is restricted by the preponderance of those of the IgG1 subclass. It is possible to selectively screen for mAbs of the rarer IgG2a and IgG2b subclasses of mouse IgGs in the process of their development and screening (24, 58). It is also possible, although labor-intensive, to manipulate hybridomas in culture and select and/or screen for subclass switched hybridoma-generated mAbs (59). However, it remains that the optimal utility of mouse mAbs in research and diagnostics is limited by the preponderance of IgG1 mAbs. Here, we have enhanced the flexibility of a substantial fraction of an existing library of widely used mouse mAbs by converting them to subclass-switched R-mAbs without altering target binding specificity. We show using mixtures of mAbs and R-mAb that we can obtain effective simultaneous multiplex labeling for combinations that were previously unattainable due to conflicting IgG subclass.

Antibody reformatting in our system is easily accomplished by the choice of plasmid backbone used for the original cloning, or by subcloning the V_L-joining fragment-V_H cassette

(Figure 1B) between plasmids with distinct C_H domains. Ultimately, one can envision using this approach to convert any mouse mAb into the corresponding set of mouse IgG1, IgG2a, and IgG2b subclass R-mAb expression plasmids. Multiplex labeling could be further expanded by constructing IgG expression vectors containing C_H regions of other species that have IgG subclasses such as rat and human (but not rabbit, in which all IgG Abs are of a generic IgG class), for which subclass-specific secondary antibodies are also widely available. For example, we interrogated the ThermoFisher secondary Ab catalog, which contains 52 different IgG subclass-specific secondary antibodies for mouse IgG subclasses, 47 for rat IgG subclasses, and 43 for human IgG subclasses. Together, the wide availability of such a broad range of reliable secondary antibodies with distinct conjugates provides ample flexibility for specific detection of multiple R-mAbs with distinct C_H regions engineered for separate detection in multiplex labeling experiments.

Previous attempts by others to generate R-mAbs have been complicated by the MOPC-21 derived aberrant kappa light chain that is present in many widely used myeloma fusion partners (22, 60-62). For example, Crosnier et al., (22) showed that depending on the hybridoma, 26% to 70% of R-mAb plasmids they generated contained this aberrant sequence. We have incorporated restriction enzyme digest of this transcript into our process to eliminate the aberrant kappa light chain (38). For most of our hybridomas, the majority of the V_L PCR product was cleaved by BciVI, indicating that the MOPC-21 aberrant light chain comprised the greatest fraction of total light chain amplicons. By eliminating this transcript, the overall screening and cloning burden for each mAb was reduced substantially. However, depending on the particular hybridoma, the efficiency of generating clones that produced functional R-mAbs even after BciVI digestion of the V_L domain PCR products was still highly variable. This was evidenced by the overall efficiency of slightly below 50% for the successful projects tabulated in Table 2, and also by the projects that were unsuccessful on the first pass in which clones passed the colony PCR and restriction digest screening steps but failed in the COS-ICC screening assay for functional R-mAbs. Moreover, a lack of allelic exclusion at heavy and light chain IgG loci has been documented in hybridomas,

527 resulting in expression of multiple IgG heavy and/or light chains at the mRNA and protein levels
528 (8-10, 63). In these previous studies, while multiple combinations of heavy and light IgG chains
529 were produced by monoclonal hybridoma cells, only one combination of heavy and light IgG
530 chains present in the hybridoma produced an R-mAb capable of recognizing the target antigen.
531 Varying degrees of allelic exclusion in the hybridomas that served as the source of our R-mAbs
532 could also contribute to the variable efficiency of whether colony PCR and restriction enzyme
533 assay-positive clones would produce an R-mAb that recapitulated immunolabeling obtained with
534 the native mAb. Technical issues, such as PCR-induced mutations may have also contributed to
535 the generation of R-mAb clones that failed in the COS-IF-ICC assay. We did not systematically
536 analyze these negative clones, so we do not know whether these plasmids contain residual
537 aberrant light chains from the BciVI digestion step, plasmids containing other heavy and/or light
538 chains, or mutated forms of *bona fide* R-mAb chains with impaired/lost functionality. That the vast
539 majority (84%) of the 114 projects for which ≥4 clones were evaluated yielded at least one positive
540 R-mAb suggests that the presence of a small and variable number of negative clones does not
541 impact the overall success of the approach described here, given the simple but effective nature
542 of microplate screening assays, such as the ICC assay employed here, to rapidly and easily
543 screen candidate R-mAbs.

544 There is a growing impetus to enhance research reproducibility by both improving the
545 quality of Abs used in basic research and in diagnostics, and the transparency of their reporting
546 as related to the exact molecularly-defined Ab that was used (1, 5, 64). Using mAbs in their
547 recombinant form and defining them unambiguously at the molecular level by publishing their V_L
548 and V_H domain sequences is a step towards achieving this goal and elevate reproducibility world-
549 wide. Among the different forms of research and diagnostic Abs, polyclonal Ab preparations have
550 unique benefits (65), due to the presence of Abs recognizing distinct epitopes on the target
551 protein. However, in any of the diverse forms in which they are available (antiserum, IgG fractions,
552 affinity-purified) polyclonal Abs are inherently limited by their intrinsic lack of precise molecular

553 definition. The inability to rigorously define the clonal composition of specific preparations can
554 contribute to batch-to-batch variation in the efficacy and specificity of the polyclonal collection for
555 any specific application, negatively impacting the reproducibility of research performed with such
556 Abs. Moreover, unlike mAbs, polyclonal Abs are a finite resource whose depletion can lead to
557 batch-to-batch variability or complete lack of availability, stymieing independent reproduction of
558 research using the same reagent. Conventional mAbs are advantageous in lacking the molecular
559 complexity of polyclonal preparations, and in being renewable reagents. However, the conversion
560 of conventional hybridoma-generated mAbs into R-mAbs offers numerous additional advantages.
561 This includes ensuring their broad availability by generating a publicly accessible DNA sequence
562 archive that can be used to synthesize the functional V_L and V_H domain sequences. R-mAbs are
563 also more easily distributed as plasmids or DNA sequence, a feature that should enhance
564 dissemination of this resource, relative to cryopreserved and living hybridomas that are
565 comparatively fragile and may not survive long-distance transport. Cloning also enhances
566 research reproducibility by the unambiguous definition of mAbs at the level of their cDNA
567 sequence, as well as the enhanced control of molecular composition afforded by expressing a
568 single light and heavy chain combination from transfected cells and their high-level animal-free
569 production in cell culture. Cloning of mAbs also allows for increased utility as offered by their
570 subsequent engineering into alternate forms, such as the subclass-switched R-mAbs generated
571 here. The method described here represents a straightforward approach to producing functional
572 R-mAbs from existing murine hybridomas that could be applied to other valuable mAb collections
573 to ensure their permanent archiving which cannot be assured when they exist solely in the form
574 of hybridomas cryopreserved in liquid nitrogen. In particular, there are many cases of important
575 hybridomas, including entire collections, that have been discarded upon the closure of the
576 laboratory that formerly housed and financially supported the maintenance of the cryopreserved
577 collection. The enhanced utility, permanence, and cost-effectiveness of R-mAbs as generated by
578 the approach described here is one route to circumvent the negative impact to research

effectiveness and reproducibility that such losses represent. Simple conversion of mAbs to R-mAbs, as described here, also paves the way for higher throughput approaches, for example those employing high throughput "next generation" sequencing to simultaneously obtain light and heavy chain sequences from large pools of hybridomas (66). In theory this should allow for larger scale "*en masse*" (as opposed to the mAb-by-mAb approach used here) conversion efforts more suitable to large hybridoma collections. For example, our larger collection of ≈40,000 target-specific mAbs archived in our cryopreserved hybridoma collection, and other widely used collections, such as that housed at the Developmental Studies Hybridoma Bank (http://dshb.biology.uiowa.edu/; comprising 3,672 mAbs as of 9/9/18) might represent appropriate targets for such next generation sequencing approaches. Future efforts to generate R-mAbs from cryopreserved hybridoma collections will further enhance the rigor, reproducibility and overall effectiveness of Ab-based research.

Materials and Methods

Primers

Primer sets for mouse Ig V region amplification and fusion PCR (F-PCR) were used as described previously (22, 25). The following primers were used for other PCR steps.

Amplification of the Joining Fragment (22)

Primer 21: 5'- GGGCTGATGCTGCACCAACTGTA-3'

Primer 26: 5'- ACTGCTTGAGGCTGGACTCGTGAACAATAGCAGC-3'

Colony PCR:

UpNotI: 5'-TTTCAGACCCAGGTACTCAT-3'

DownAscI: 5'-GGGCAGCAGATCCAGGGGCC-3' (reverse primer for IgG1 vector)

Rev IgG2a: 5'- ACCCTTGACCAGGCATCCTAGAGT- 3' (reverse primer for IgG2a vector)

Mouse γ2a C_H domain amplification (restriction sites are underlined):

IgG2a-F-AscI: 5'-ATATCACGGCGCGCCCAACAGCCCCATCGGTCTATCCA-3'

IgG2a-R-XbaI: 5'GACTGATCTAGAATCATTTACCCGGAGTCCGGGAGAA-3'

R-mAb Sequencing:

Forward strand of V_L region: UpNotI = 5'-TTTCAGACCCAGGTACTCAT-3'

Reverse strand of V_L region (IgG2a plasmids): Seq_VL_Rev_IgG2a = 5' -CCAACTGTTCAGGACGCCATT -3'

Forward strand of VH region: VH_seq_Forward = 5'- TCCCAGGCCACCATGAA -3'

Reverse strand of V_H region (IgG1 plasmids): DownAscI = 5'-GGGCAGCAGATCCAGGGGCC-3'

Reverse strand of V_H region (IgG2a plasmids): Rev IgG2a = 5'-ACCCTTGACCAGGCATCCTAGAGT- 3'

RNA preparation from cryopreserved hybridomas and RT-PCR

The Ambion RNAqueous 96 Extraction kit (Thermo Fisher Cat# AM1920) was used for high throughput RNA extraction. Frozen vials containing 0.5-1 x 10^7 hybridoma cells per vial were thawed in a 37ºC water bath for 5 minutes, in batches of 20 vials for high through-put purposes. Cells were spun down in a table top centrifuge at 2000 rpm for 5 min, the supernatant was removed, and cells were washed with 1 mL cold PBS. A 250 µL aliquot of this cell suspension was used for RNA extraction according to the manufacturer's instructions. The Superscript III Reverse Transcriptase First Strand Synthesis System (Thermo Fisher Cat# 18080051) was used for high throughput cDNA synthesis in 96 well plates using 4.0 µL of RNA per reaction and oligo (dT) primers.

Immunoglobulin V Region Amplification, BciVI Treatment, and Fusion PCR

Amplification of Ig V region sequences and fusion PCR (F-PCR) to join V_L and V_H PCR products were performed as described (22, 25) with the noted modifications. Briefly, degenerate primer sets were used to amplify mouse Ig kappa V_L and V_H sequences using 1.0 µL of 10-fold diluted, hybridoma-derived cDNA as a template. PFU Ultra II Fusion HS DNA polymerase (Agilent Technologies Cat# 600670) and Advantage 2 Polymerase Mix (ClonTech Cat# 639201) were used for V_L and V_H amplification, respectively. PCR conditions for V_L amplification were: 95ºC for 5 minutes; 5 cycles of 95ºC for 20 s, 60ºC for 20 s, 72ºC for 30 s; 19 cycles of 95ºC for 20 s, 60.5ºC for 20 s with 0.5ºC decrement per cycle, 72ºC for 30 s; 10 cycles of 95ºC for 20 s, 55ºC for 20 s, 72ºC for 30 s; 72ºC for 15 min. PCR conditions for V_H amplification were: 95ºC for 5 minutes; 5 cycles of 95ºC for 45 s, 62ºC for 30 s, 72ºC for 1 min; 19 cycles of 95ºC for 45 s, 64.5ºC for 30 s with 0.5ºC decrement per cycle, 72ºC for 1 min; 10 cycles of 95ºC for 45 s, 55ºC for 30 s, 72ºC for 1 min; 72ºC for 15 min. V_L PCR products (7.0 µL per reaction) were digested with 5 units of the restriction enzyme BciVI (BfuI) (Thermo Fisher Cat# ER1501) in a 20 µL reaction at 37ºC for 2 hrs. The enzyme was inactivated by heating to 80ºC for 20 min.

In preparation for fusion of the V_L and V_H PCR products, a joining fragment was produced using the mouse Ig expression plasmid P1316 (a gift of Dr. Gavin Wright, Sanger Institute, Cambridge, UK, now available from Addgene as plasmid #28217). The joining fragment contains the following sequences (5' to 3'): mouse kappa light chain constant region, a polyadenylation signal, a CMV promoter, and the leader sequence for the Ig heavy chain. P1316 was used as a template in a 50 µL PCR containing 0.2 µM of primers 21 and 26, 0.2 mM dNTPs, and 1.0 µL PFU Ultra II Fusion HS DNA polymerase. PCR conditions were: 95ºC for 5 min; 5 cycles of 95ºC for 20 s, 60ºC for 20 s, 72ºC for 45 s; 19 cycles of 95ºC for 20 s, 60.5ºC for 20 s with 0.5ºC decrement per cycle, 72ºC for 45 s; 10 cycles of 95ºC for 20 s, 55ºC for 20 s, 72ºC for 45 s; 72ºC for 15 min. The 1.7 kb joining fragment was purified (Qiagen/QiaQuick PCR Purification Cat# 28106) in preparation for F-PCR.

657 V_L (BciVI restriction enzyme digested), the joining fragment, and V_H PCR products were
658 joined via F-PCR in a 96-well format. We observed that purification of V_L and V_H PCR products
659 was not necessary. Each 50 µL reaction consisted of the following: 0.2 µM of primers 51 and 52
660 (22, 25), 0.2 mM dNTPs, 1.5 µL V_L (BciVI digested), 0.5 µL V_H, 0.5 µL purified joining fragment
661 (50 ng), and 1.0 µL PFU Ultra II Fusion HS DNA polymerase. PCR conditions were: 95ºC for 2
662 minutes; 11 cycles of 95ºC for 45 s, 63ºC for 30 s, 72ºC for 5 min; 7 cycles of 95ºC for 45 s, 62ºC
663 for 30 s with 1ºC decrement per cycle, 72ºC for 5 min, 95ºC for 45 s; 26 cycles of 56ºC for 30 s,
664 72ºC for 5 min; 72ºC for 15 min.
665
666 **Cloning of Immunoglobulin Variable Domain Regions into a Dual Promoter Expression**
667 **Plasmid**
668 F-PCR products were digested with FastDigest NotI and AscI (Thermo Fisher Cat#
669 ER0595 and ER1891, respectively) at 37ºC for 20 min, followed by inactivation at 80ºC for 5 min
670 and column purification (Qiagen/QiaQuick PCR Purification Cat# 28106). The P1316 plasmid was
671 also NotI/AscI digested and gel purified (Qiagen/QiaQuick Gel Extraction Cat# 28706). P1316 is
672 a derivative of the pTT3 expression vector (26) and consists of (5' to 3'): a CMV promoter, the
673 mouse V kappa leader sequence, a NotI restriction site, an insert consisting of V_L/joining
674 fragment/V_H, and the mouse IgG1 C_H sequence amplified from mouse genomic DNA, flanked by
675 AscI and XbaI restriction sites (22, 25). Ligation was performed overnight at 16ºC with T4 DNA
676 ligase (Thermo Fisher Cat# 15224017) using 20 ng insert and 20 ng vector, a 3:1 molar ratio. Half
677 of each ligation reaction was used to transform 25 µL of Mach I chemically competent *E. coli.*
678 (Thermo Fisher Cat# C862003). Cells and DNA were incubated on ice for 30 min, heat shocked
679 at 42ºC for 30 s, incubated on ice for 2 min, and allowed to recover for 1.0 hr in 250 µL SOC
680 medium in a 37ºC shaking incubator. The cells were spun in a centrifuge at 3000 rpm (≈950 x g)
681 for 2 min and the supernatant was removed until 150 µL remained. Cells were resuspended, and

682 the entire volume was plated on LB plates containing 100 µg/mL ampicillin and incubated
683 overnight at 37ºC.
684
685 **Colony PCR, Restriction Analysis and Sequencing of R-mAb Clones**
686 Colony PCR was performed to identify *E. coli* colonies that contained the full-length, 2.4
687 kb Ig cassette. Colonies were diluted in 96-well plates containing 50 µL water and patch plates
688 were made for later recovery of positive clones. 2 µL of diluted colony was used in each PCR.
689 Conditions were 94°C for 5 min; 23 cycles of 94°C for 20 s, 58°C for 30 s, 72°C for 2.5 min; 72°C
690 for 10 min. For additional confirmation of the presence of the full-length Ig cassette, plasmid DNA
691 was isolated from PCR positive clones and subjected to restriction enzyme digestion with
692 NotI/AscI at 37ºC for 20 min followed by agarose gel electrophoresis. The V_L and V_H regions of
693 functional R-mAbs were subjected to sequencing in both orientations to generate a permanent
694 archive. The primers “UpNotI” and “Seq_VL_Rev_IgG2a” were used for V_L domain sequencing,
695 and the “VH seq forward”, and either “DownAscI” or “Rev IgG2a” for sequencing of V_H regions in
696 the IgG1 or IgG2a expression plasmids, respectively.
697
698 **Generation of a mouse IgG2a expression vector**
699 The mouse γ2a C_H domain was amplified from the cDNA preparation that was obtained
700 from the K28/43 (RRID: AB_2292909) hybridoma (27, 28) that was used for cloning of the K28/43
701 V_L and V_H domains. PCR conditions were: 94ºC for 5 min; 29 cycles of 94ºC for 30 s, 65ºC for 30
702 s, 72ºC for 30 s. The forward primer included an AscI restriction site and the reverse primer
703 included an XbaI restriction site to facilitate cloning into the K28/43 IgG1 recombinant R-mAb
704 plasmid. The K28/43 IgG1 recombinant R-mAb plasmid was derived from the P1316 plasmid (22)
705 by restriction enzyme-based cloning of K28/43 variable region sequences as described above.
706 The IgG2a C_H PCR product and the K28/43 IgG1 recombinant plasmid were both digested with
707 AscI and XbaI restriction enzymes (New England BioLabs Cat# R0558 and R0145, respectively)

and column purified (Qiagen/QiaQuick PCR Purification Cat# 28106) or agarose gel purified, respectively (Qiagen/QiaQuick Gel Extraction Cat# 28706). Because XbaI is methylation sensitive, the K28/43 IgG1 plasmid was sourced from *dam*$^{-}$*/dcm*$^{-}$ *E. coli* (New England Biolabs Cat# C2925). T4 DNA ligase (New England Biolabs Cat# M0202) was used to insert the IgG2a C_H fragment into the digested K28/43R plasmid to generate a K28/43 IgG2a R-mAb plasmid which was confirmed by DNA sequencing.

R-mAb Expression in Mammalian Cells

For production of recombinant mAbs in mammalian cell culture, 3 x 10^5 COS-1 cells were plated on 35 mm tissue culture dishes and cultured overnight in DMEM (high glucose/pyruvate, Thermo Fisher Cat# 11995065) with 10% Fetal Clone III (HyClone Cat# SH30109.03) and 100 µg/ml penicillin/streptomycin (Thermo Fisher Cat# 15140122). Cells were then transfected with a 1:1 ratio of plasmid (1 µg):Lipofectamine 2000 (1 µL) (Thermo Fisher Cat# 11668019) diluted in Opti-MEM reduced serum medium (Thermo Fisher Cat# 31985070). Following an overnight incubation, the transfection solution was replaced with culture medium, and the cells incubated for an additional six days, at which time the conditioned medium was collected as R-mAb tissue culture supernatant (TC supe) for analysis.

COS Cell Immunofluorescence Immunocytochemistry Validation Assay

R-mAb TC supes were screened for immunoreactivity in an immunofluorescence assay against transiently transfected COS-1 cells cultured in 96-well plates. COS-1 cells were plated in black, clear bottom 96-well plates (Greiner Cat# 655090) at a density of 4,700 cells/well. After overnight incubation, each well received 50 ng plasmid DNA encoding the R-mAb target protein plus Lipofectamine 2000 at a 1:1 ratio as described above. On day 3 post-transfection, cells were washed 3 times with DPBS (138 mM NaCl, 2.67 mM KCl, 1.47 mM KH_2PO_4, 8.1 mM Na_2HPO_4, 1 mM $CaCl_2$ and 1 mM $MgCl_2$), pH 7.4 and then fixed using 3.0% formaldehyde (prepared fresh

from paraformaldehyde) in in DPBS plus 0.1% Triton X-100 on ice for 20 min. Cells were washed 3 times with DPBS/0.1% Triton X-100, blocked with Blotto/0.1% Triton X-100 for 1 hr, and stored in DPBS/0.02% sodium azide. For primary antibody labeling, R-mAb TC supes were used without dilution and hybridoma-generated mAb TC supe controls (see Table 4 for details of non-R-mAb Abs used in this study) were diluted 1:10 in COS-1 cell culture medium. Each R-mAb was tested alone and in combination with the corresponding hybridoma-generated mAb TC supe. Primary antibodies were incubated at room temperature for 1 hr and cells were washed 3 x 10 min with Blotto/0.1% Triton X-100. Secondary labeling was performed at room temperature for 30 min using subclass-specific, anti-mouse secondary antibodies conjugated to Alexa Fluors (Thermo Fisher, Cat#/IgG subclass/Alexa Fluor dye conjugates: (A-21121/IgG1/488 and A-21241/IgG2a/647) and diluted to 1.3 µg/mL in Blotto/0.1% Triton X-100. Hoechst 33342 (Thermo Fisher Cat# H3570) was used at 0.1 µg/mL in the secondary antibody cocktail to stain nuclear DNA. Cells were washed 3 x 10 min with DPBS/0.1% Triton X-100. Imaging was performed using a Zeiss M2 AxioImager microscope. Images were processed using Zeiss Axiovision and ImageJ software.

For higher resolution imaging, COS-1 cells were plated on poly-L-lysine coated #1.5 glass cover slips and cultured overnight followed by transfection with plasmids encoding the target protein. Cells were fixed and immunolabeled as described in the previous section. Images were acquired on a Zeiss AxioImager M2 microscope using a 40x/0.8 NA plan-Apochromat oil-immersion objective and an AxioCam MRm digital camera. Optical sections were acquired using an ApoTome 2 structured illumination system (Carl Zeiss MicroImaging). Imaging and post processing were performed in Axiovision (Carl Zeiss MicroImaging) and Photoshop (Adobe Systems).

Multiplex immunofluorescence labeling of immunoblots

Multiplex immunofluorescence labeling of immunoblots using mouse IgG subclass-specific secondary antibodies was performed as described previously (18). In brief, samples were generated from COS-1 cells transiently transfected to express individual target proteins essentially as described above for the immunofluorescence experiments except that the cells were cultured in 35 mm tissue cultures dishes. Transfected COS-1 cells were washed once with ice-cold PBS and lysed with 150 µL of ice-cold lysis buffer containing 1% v/v Triton X-100, 150 mM NaCl, 1 mM EDTA, 50 mM Tris-HCl (pH 7.4), 1 mM sodium orthovanadate, 5 mM NaF, 1 mM PMSF and a protease inhibitor cocktail for 10 min at 4ºC (29). The cell lysates were centrifuged at 12,000 x g at 4 ˚C for 10 min. The cell lysate supernatants were mixed with 150 µL of 2X RSB and size-fractionated by 7.5% SDS–PAGE. Following SDS-PAGE, proteins were transferred to nitrocellulose membranes (Bio-Rad Cat# 1620115), which were blocked for 1 h with Blotto (3% w/v nonfat milk in Tris-buffered saline (TBS: 50 mM Tris, pH 7.5, 150 mM NaCl) plus 0.1% v/v Tween-20 followed by 2 h or overnight incubation with primary antibodies. Primary antibodies were mAb TC supes diluted 1:10, non-diluted R-mAb TC supes, and an in-house anti-PSD-95 rabbit polyclonal antibody raised against a GST fusion protein, GSTKAP1.13, containing amino acids 77–299 of human PSD-95 [clone 2, (30)] and that crossreacts with SAP97 (see Table 4 for details of non-R-mAb Abs used in this study). After 3 washes with Blotto, the membranes were incubated with the appropriate subclass-specific Alexa Fluor conjugated secondary antibodies (18) for 1 h. After 3 washes with TBS containing 0.1% v/v Tween-20, the immunoblots were visualized directly on a FluorChem Q imager (Cell Biosciences Cat# DE500-FCQ). Alternatively, crude rat brain membranes (RBM) (29) were subjected to immunoblotting as described above except that a single RBM sample (3 mg protein) were size fractionated on a curtain gel, and after transfer to nitrocellulose the membrane was cut into 30 strips, each containing 100 µg of RBM protein. Immunolabeling was detected on autoradiography film after treatment of strip

785 immunoblots with HRP-conjugated anti-mouse IgG-specific secondary antibody and enhanced
786 chemiluminescence (ECL).
787
788 **Multiplex immunofluorescence labeling of brain sections**
789 Multiplex immunofluorescence labeling of brain sections was performed essentially as
790 described previously (18, 31). All experimental procedures were approved by the UC Davis
791 Institutional Animal Care and Use Committee and conform to guidelines established by the
792 National Institutes of Health (NIH). Rats were anesthetized with sodium pentobarbital (Fatal-Plus
793 solution, 100 mg/kg sodium pentobarbital) and perfused transcardially with 100 mL of phosphate
794 buffered saline (PBS), containing 10 units/mL heparin, pH 7.4, followed by 400 mL of 4%
795 formaldehyde (prepared fresh from paraformaldehyde) in 0.1 M sodium phosphate buffer or PB
796 (pH 7.4). The brains were removed, cryoprotected for 48 hr in 30% sucrose, frozen in a bed of
797 pulverized dry ice, and then cut into 30 µm sections on a freezing-stage sliding microtome.
798 Sections were collected in 0.1 M PB and processed immediately for immunohistochemistry. Free-
799 floating brain sections were blocked with 10% goat serum in 0.1 M PB containing 0.3% Triton X-
800 100 (vehicle) for 1 h at RT and then incubated overnight at 4°C in vehicle containing different
801 combinations of primary antibodies (see Table 4 for details of non-R-mAb Abs used in this study).
802 The following day sections were washed 4 X 5 min each with vehicle, and then incubated for 1 h
803 at RT in mouse IgG subclass-specific or anti-rabbit Alexa-conjugated secondary antibodies as
804 described previously (18, 32). Sections were then washed 2 X 5 min each with 0.1 M PB, 2 X 5
805 min each with 0.05 M PB and mounted on gelatin-coated microscope slides and air dried. Sections
806 were cover slipped after adding ProLong Gold Antifade Mountant (Thermo Fisher Scientific
807 catalog # P36930). Images were obtained on a Zeiss Axiovert 200 microscope with Apotome.
808 Imaging and post-imaging processing was performed in Zeiss Axiovision and Adobe Photoshop
809 software, taking care to maintain any linear differences in signal intensities present in the original
810 samples.

811 **Table 1. Aberrant V_L sequences remaining after BciVI digestion**

812

mAb	Number of clones sequenced	Number of clones with aberrant chain	% with aberrant chain
K7/45	5	0	0
K9/40	7	2	28.6
K13/31	10	0	0
K14/16.2	2	0	0
K14/16.2.1	9	2	22.2
K17/70	6	1	16.7
K28/86	3	0	0
K36/15	6	1	16.7
K74/71	6	0	0
K75/41	3	0	0
K87A/10	3	0	0
L6/60	3	0	0
L21/32	4	0	0
L23/27	6	0	0
L61/14	7	1	14.3
N59/20	2	2	100
N70/28	1	0	0
N86/8	8	2	25.0
N86/38	22	0	0
N100/13	6	0	0
N103/31	4	1	25.0
N103/39	5	0	0
N105/13	5	0	0
N106/36	6	0	0
N116/14	3	0	0
N297/59	7	0	0
Total	149	12	8.1

813

814

815 **Table 2. Conversion efficiency of a selected subset of R-mAbs**

816

Successful Projects (130 total)				Unsuccessful Projects (51 total)	
BciVI-resistant (129 total)				BciVI-resistant	
mAb	Colony PCR/Restriction Digest Positives	COS-ICC Positives	% Positive	mAb	Colony PCR/Restriction Digest Positives
D3/71	12	3	25.0	K67/25	2
K7/45	3	1	33.3	K73/20	1
K13/31	3	1	33.3	K78/29	3
K14/16	1	1	100.0	L23/27	3
K19/36	4	3	75.0	L24/18	8
K20/78	6	2	33.3	L48A/9	1
K25/73	8	5	62.5	L57/46	3
K28/86	1	1	100.0	L58A/6	3
K36/15	4	2	25.0	L60/6	2
K37/89	2	1	50.0	L71/5	5
K39/25	5	2	40.0	L76/36	5
K47/42	1	1	100.0	L92/69	6
K51/1	2	1	50.0	L92/70	10
K55/7	5	3	60.0	L92/89	9
K56A/50	4	3	75.0	N18/28	5
K57/1	4	2	50.0	N38/8	6
K64/15	4	3	75.0	N64A/36	1
K66/38	4	3	75.0	N68/6	15
K72/8	3	1	33.3	N71/37	4
K75/41	5	1	20.0	N81/2	5
K91/36	7	3	42.9	N86/8	2
K96/7	2	2	100.0	N86/44	4
L5/1	1	1	100.0	N87/25	3
L8/15	1	1	100.0	N92/14	4

L18A/3	7	2	28.6
L20/8	10	1	10.0
L21/32	11	7	63.6
L42/17	11	4	36.4
L43/40	6	2	33.3
L45/30	9	1	11.1
L51/82	2	1	50.0
L60/4	8	3	37.5
L61/14	4	2	50
N2/16	4	3	75.0
N3/26	8	1	12.5
N6/38	4	1	25.0
N7/18	5	3	60.0
N11/33	13	2	15.4
N15/4	2	1	50.0
N16B/8	3	3	100.0
N18/30	11	3	27.3
N23B/49	2	2	100.0
N28/9	7	4	57.1
N29/29	8	4	50.0
N34/34	3	1	33.3
N50/36	5	1	20.0
N51/6	4	2	50.0
N52A/42	9	4	44.4
N59/36	5	1	20.0
N70/28	3	1	33.3
N77/15	5	1	20.0
N81/37	6	4	66.7
N83/48	4	1	25.0
N84/37	6	4	66.7
N85/18	5	2	40.0
N85/37	6	4	66.7
N86/38	4	2	50.0
N87/25	4	2	50.0
N88/12	6	5	83.3
N93A/49	6	1	16.7
N94/17	6	2	33.3

N95/35	2
N97A/31	2
N105/17	5
N119/44	1
N121A/1	2
N125/10	2
N129/15	3
N134/12	3
N141/28	1
N142/28	5
N144/17	2
N144/32	3
N170A/26	3
N173B/13	4
N183/15	1
N209C/35	3
N212A/34	1
N308/48	6
N319/14	1
N326D/13	2
N330A/80	2
N356/9	2
N363/71	2
N388A/27	3
N399/19	2
N408/79	1
N422/18	4
Total	**178**

N96/55	6	5	83.3
N104/32	5	2	40.0
N110/29	5	2	40.0
N111/24	3	1	33.3
N112B/14	4	1	25.0
N116/14	7	3	42.9
N117/9	8	5	62.5
N121A/31	6	4	66.7
N124B/38	3	2	66.7
N127/31	9	8	88.9
N129A/6	6	2	33.3
N133/21	4	2	50.0
N135/37	7	1	14.3
N147/6	3	2	66.7
N164/6	2	1	50.0
N168/6	4	1	25.0
N170A/1	5	1	20.0
N171/17	8	2	25.0
N174B/27	3	3	100.0
N176A/35	2	1	50.0
N178A/9	4	2	50.0
N180/41	3	2	66.7
N195A/16	11	3	27.3
N196/16	6	3	50.0
N201/35	2	2	100.0
N205B/22	2	1	50.0
N206A/8	10	1	10.0
N206B/9	7	5	71.4
N212/3	7	4	57.1
N212/7	4	1	25.0
N212/17	8	4	50.0
N222/6	11	4	36.4
N229A/32	8	8	100.0
N230/21	8	3	37.5
N235/22	9	7	77.8
N244/5	7	2	28.6
N268/19	8	1	12.5

N269/73	10	5	50.0
N271/44	2	1	50.0
N277/7	9	2	22.2
N278/19	3	1	33.3
N279B/27	10	10	100.0
N289/16	3	3	100.0
N291C/22	7	5	71.4
N295B/54	5	2	40.0
N295B/66	10	5	50.0
N320/48	9	6	66.7
N321C/49	2	1	50.0
N323B/20	6	4	66.7
N325B/65	4	1	25.0
N326D/29	11	10	90.9
N328B/37	10	2	20.0
N331/19	10	3	30.0
N341/37	6	2	33.3
N346/9	2	2	100.0
N348/82	8	4	50.0
N353/13	6	2	33.3
N355/1	7	4	57.1
N356/23	10	7	70.0
N359/28	7	6	85.7
N388A/10	4	2	50.0
N388A/60	8	1	12.5
N398A/34	11	11	100.0
N413/67	1	1	100.0
N415/24	6	4	66.7
N419/40	13	10	76.9
N419/78	3	1	33.3
1F1	9	4	44.4
Total	**741**	**359**	**48.4**
BciVI-sensitive			
K58/35	19	7	36.8

817

818 **Table 3. mAbs converted to validated R-mAbs**

819

Clone	Target	mAb IgG subclass	R-mAb IgG subclass	mAb RRID	R-mAb RRID
1F1	TrpC1	IgG1	IgG2A	AB_10999751	AB_2750650
D3/71	Kv2.1 K+ channel	IgG1	IgG2A		AB_2750651
K7/45	Kv1.5	IgG1	IgG2A	AB_10675288	AB_2750674
K9/40	Kvbeta1.1 K+ channel	IgG2b	IgG2A	AB_10672857	AB_2750678
K13/31	Kv1.4 K+ channel	IgG1	IgG2A	AB_10673576	AB_2750652
K14/16	Kv1.2 K+ channel	IgG2b	IgG2A	AB_10674277	AB_2750653
K17/70	Kvbeta2 K+ channel	IgG1	IgG2A	AB_10673520	AB_2750654
K19/36	Kv1.6 K+ channel	IgG3	IgG2A	AB_10671825	AB_2750655
K20/78	Kv1.1 K+ channel	IgG1	IgG2A	AB_10672854	AB_2750656
K25/73	Pan-Kvbeta K+ channel	IgG1	IgG2A	AB_2336914	AB_2750657
K28/43	PSD-95	IgG2a	IgG1	AB_10698024	AB_2750658
K28/43	PSD-95	IgG2a	IgG2A	AB_10698024	AB_2750659
K28/86	Pan-MAGUK	IgG1	IgG2A	AB_10698179	AB_2750660
K36/15	Kv1.1 K+ channel (external)	IgG2b	IgG2A	AB_10673166	AB_2750661
K37/89	Kv2.2 K+ channel	IgG2a	IgG2A	AB_10673393	AB_2750662
K39/25	Kv2.1 K+ channel (external)	IgG2a	IgG2A	AB_10674578	AB_2750663
K40/17	Pan-Kvbeta K+ channel	IgG2a	IgG2A	AB_10672417	AB_2750664
K47/42	Kvbeta1.2 K+ channel	IgG1	IgG2A	AB_10671827	AB_2750665
K51/1	SH3GL1/Endophilin A2	IgG1	IgG2A	AB_10698030	AB_2750666
K55/7	KChIP1 K+ channel	IgG1	IgG2A	AB_10697876	AB_2750667
K55/82	KChIP1 K+ channel	IgG2a	IgG2A	AB_2132595	AB_2750668
K56A/50	CASK	IgG1	IgG2A	AB_10671954	AB_2750669
K57/1	Kv4.2 K+ channel (external)	IgG1	IgG2A	AB_10672254	AB_2750670
K58/35	pan-Nav	IgG1	IgG2A	AB_477552	AB_2750671
K64/15	SAP97	IgG1	IgG2a	AB_10672989	AB_2750672
K66/38	KChIP3 K+ channel	IgG2a	IgG2a	AB_10697878	AB_2750673
K72/8	Co-Rest/RCOR1	IgG1	IgG2A	AB_10673564	AB_2750675
K75/41	Kv4.3 K+ channel	IgG1	IgG2A	AB_10672856	AB_2750676
K89/34	Kv2.1 K+ channel	IgG1	IgG2A	AB_10672253	AB_2750677
K91/36	WAVE1/SCAR	IgG1	IgG2A	AB_10671317	AB_2750679

K96/7	Pancortin	IgG1	IgG2A	AB_10674112	AB_2750680
L5/1	SCG10/Stathmin-2	IgG2b	IgG2A	AB_10671663	AB_2750688
L6/23	Slo1/BKAlpha maxi-K+ channel	IgG1	IgG2A	AB_2493094	AB_2750690
L8/15	Snapin/SNAPAP	IgG1	IgG2A	AB_10675326	AB_2750694
L18A/3	BKbeta4 K+ channel	IgG2a	IgG2A	AB_10675133	AB_2750681
L20/8	PICK1	IgG2a	IgG2A	AB_10672986	AB_2750682
L21/32	GluA2/GluR2 glutamate receptor	IgG1	IgG2A	AB_10674575	AB_2750683
L28/4	Kv4.2 K+ channel	IgG1	IgG2A	AB_2315873	AB_2750684
L42/17	SynDIG1/Tmem90b	IgG2a	IgG2A	AB_11000166	AB_2750685
L43/40	DLX1	IgG2a	IgG2A	AB_10671701	AB_2750686
L45/30	SynCAM1	IgG1	IgG2A	AB_10671665	AB_2750687
L51/82	MMP9	IgG2a	IgG2A	AB_10672974	AB_2750689
L60/4	Copper ATPase 1 (Menke's disease protein)	IgG2b	IgG2A	AB_10672736	AB_2750691
L61/14	Kv2.1 K+ channel pS603	IgG1	IgG2A	AB_2315769	AB_2750692
L62/29	Copper ATPase 2 (Wilson's disease protein)	IgG1	IgG2A	AB_10672737	AB_2750693
L80/21	Kv2.1 K+ channel	IgG3	IgG2A	AB_2315862	AB_2750695
N2/16	KCNU1/Slo3 maxi-K+ channel	IgG1	IgG2A	AB_10698181	AB_2750743
N3/26	KCNT1/Slo2.2/Slack K+ channel	IgG1	IgG2A	AB_10698032	AB_2750772
N6/38	VAChT	IgG1	IgG2A	AB_10674274	AB_2750807
N7/18	Cavbeta1 Ca2+ channel	IgG2a	IgG2A	AB_10673098	AB_2750809
N8B/1	Cavbeta2 Ca2+ channel	IgG1	IgG2A	AB_10675135	AB_2750822
N10/7	Cavbeta4 Ca2+ channel	IgG1	IgG2A	AB_10671176	AB_2750696
N11/33	KCNT2/Slo2.1/Slick K+ channel	IgG1	IgG2A	AB_10675450	AB_2750700
N15/4	TrpV3	IgG2a	IgG2A	AB_10675455	AB_2750722
N15/39	TrpV3	IgG1	IgG2A	AB_10675456	AB_2750721
N16B/8	Kv3.1b K+ channel	IgG1	IgG2A	AB_10672409	AB_2750730
N18/30	PSD-93/Chapsyn-110	IgG1	IgG2A	AB_10673100	AB_2750737
N19/2	SAP102	IgG1	IgG2A	AB_10671660	AB_2750740
N22/21	Shank1	IgG1	IgG2A	AB_10673108	AB_2750751
N23B/6	Shank2	IgG1	IgG2A	AB_10674119	AB_2750757
N23B/49	Pan-Shank	IgG1	IgG2A	AB_10674115	AB_2750756
N26A/23	Kv7.2/KCNQ2 K+ channel	IgG1	IgG2A	AB_10673164	AB_2750761
N28/9	VGlut1	IgG1	IgG2A	AB_10673111	AB_2750766

N29/29	VGlut2	IgG1	IgG2A	AB_10698039	AB_2750768
N34/34	VGlut3	IgG1	IgG2A	AB_10698040	AB_2750780
N37A/10	Kv7.1/KCNQ1 K+ channel	IgG1	IgG2A	AB_10675286	AB_2750788
N40B/18	BKbeta3a K+ channel	IgG1	IgG2A	AB_10673961	AB_2750792
N49A/21	NGL-1/LRRC4C	IgG1	IgG2A	AB_10671309	AB_2750797
N50/36	NGL-2/LRRC4	IgG1	IgG2A	AB_10697883	AB_2750798
N51/6	NGL-3/LRRC4B	IgG1	IgG2A	AB_10672415	AB_2750799
N52A/42	Mortalin/GRP75	IgG1	IgG2A	AB_10674108	AB_2750800
N52B/27	SALM2/LRFN1	IgG1	IgG2A	AB_10674118	AB_2750801
N53/32	BKbeta2 K+ channel	IgG2a	IgG2A	AB_10674434	AB_2750802
N55/10	Cav3.2 Ca2+ channel	IgG1	IgG2A	AB_2315825	AB_2750803
N56/21	FGF14/FHF4	IgG1	IgG2A	AB_10671703	AB_2750804
N57/2	ADAM22 (extracellular)	IgG1	IgG2A	AB_10671172	AB_2750805
N59/36	GluN2B/NR2B glutamate receptor	IgG2b	IgG2a	AB_10672980	AB_2750806
N69/46	Shank3	IgG2b	IgG2a	AB_10698031	AB_2750808
N70/28	HCN1	IgG1	IgG2A	AB_10672848	AB_2750810
N75/3	mGluR1/5 (Group I) glutamate receptor	IgG2a	IgG2A	AB_10672304	AB_2750811
N76/3	Ataxin-1, 11NQ	IgG1	IgG2A	AB_10673969	AB_2750812
N76/8	Ataxin-1, 11NQ	IgG2b	IgG2A	AB_10671173	AB_2750813
N77/15	TrpC4	IgG2b	IgG2A	AB_10698036	AB_2750814
N81/37	GABA(B)R2	IgG1	IgG2A	AB_10672297	AB_2750815
N83/48	GIT2	IgG1	IgG2A	AB_10672302	AB_2750816
N84/37	Laforin	IgG1	IgG2A	AB_10673395	AB_2750817
N85/18	Malin	IgG1	IgG2A	AB_10673396	AB_2750818
N86/38	GFP	IgG2a	IgG2a	AB_10671955	AB_2750819
N87/25	GABA(A)R, Beta3	IgG1	IgG2a	AB_10673389	AB_2750820
N88/12	MESD	IgG2b	IgG2A	AB_10673280	AB_2750821
N91/27	FGF13/FHF2	IgG1	IgG2A	AB_10675138	AB_2750823
N93A/49	GABA(B)R1	IgG1	IgG2A	AB_10672843	AB_2750824
N94/17	FGF12/FHF1	IgG1	IgG2A	AB_10675137	AB_2750825
N96/55	GABA(A)R, Beta1	IgG1	IgG2A	AB_10673157	AB_2750826
N97A/31	Neuroligin-1	IgG1	IgG2A	AB_10671307	AB_2750827
N98/7	Neuroligin-4*	IgG1	IgG2A	AB_2151948	AB_2750828
N103/39	Aldh1L1 (blotting)	IgG1	IgG2A	AB_10673447	AB_2750697
N104/32	SNAT1	IgG1	IgG2A	AB_10674120	AB_2750698
N106/20	Ankyrin-G (blotting)	IgG1	IgG2A	AB_10674433	AB_2750699

N110/29	Neuroligin-3	IgG1	IgG2A	AB_10673403	AB_2750701
N111/24	Mitofusin-1	IgG1	IgG2A	AB_10675293	AB_2750702
N112B/14	Kir2.1 K+ channel	IgG1	IgG2A	AB_11001668	AB_2750703
N114/10	HCN4	IgG1	IgG2A	AB_10673158	AB_2750704
N116/14	Botch	IgG1	IgG2A	AB_10671697	AB_2750705
N117/9	DNMT3L	IgG1	IgG2A	AB_10673155	AB_2750706
N120A/9	Neuregulin-HBD (Heparin binding domain, Type I/II)	IgG2a	IgG2A	AB_2154679	AB_2750707
N121A/31	Pannexin-2	IgG1	IgG2A	AB_10673509	AB_2750708
N123/19	Histone H3-pThr11	IgG1	IgG2A	AB_10673569	AB_2750709
N124B/38	Kir2.2 K+ channel	IgG1	IgG2A	AB_10697879	AB_2750710
N127/31	Pan-SAPAP	IgG2b	IgG2A	AB_10697886	AB_2750711
N129A/6	Mad3	IgG2b	IgG2A	AB_10674581	AB_2750712
N133/21	RGS14	IgG2a	IgG2A	AB_10698026	AB_2750713
N135/37	JIP-2/IB-2	IgG1	IgG2A	AB_10672307	AB_2750714
N138/6	LRRK2/Dardarin	IgG1	IgG2A	AB_10697869	AB_2750715
N144/14	6xHis	IgG1	IgG2A	AB_10671171	AB_2750716
N144/17	Gamma-protocadherin-A3	IgG1	IgG2A	AB_10697874	AB_2750717
N145/20	Pan-GRK	IgG1	IgG2A	AB_10671656	AB_2750718
N147/6	Pan-QKI	IgG2b	IgG2A	AB_10671658	AB_2750719
N149/25	Olig1	IgG1	IgG2A	AB_10674111	AB_2750720
N150/21	Doc2b	IgG1	IgG2A	AB_2277497	AB_2750723
N151/3	GABA(A)R, Delta	IgG2a	IgG2A	AB_10672295	AB_2750724
N153/5	Mitofusin-2	IgG2a	IgG2A	AB_10672973	AB_2750725
N155/9	Uncx	IgG1	IgG2A	AB_10672528	AB_2750726
N160/21	SynDIG3/Tmem91	IgG2b	IgG2A	AB_10676102	AB_2750727
N164/6	LRP4 (cytoplasmic)	IgG1	IgG2A	AB_10672256	AB_2750728
N168/6	Navbeta4 Na+ channel	IgG1	IgG2A	AB_10673578	AB_2750729
N170A/1	Neurexin-1-Beta	IgG1	IgG2A	AB_10672978	AB_2750731
N170A/26	Neurexin-1-Beta	IgG1	IgG2A	AB_10674585	AB_2750732
N171/17	INPP4b	IgG1	IgG2A	AB_2296057	AB_2750733
N174B/27	Gamma-protocadherin-C3	IgG1	IgG2A	AB_10675141	AB_2750734
N176A/35	S100A5	IgG1	IgG2A	AB_2183799	AB_2750735
N178A/9	Cav3.1 Ca2+ channel	IgG1	IgG2A	AB_10673097	AB_2750736
N180/41	EAAC1	IgG1	IgG2A	AB_10697871	AB_2750738
N182/17	QKI-6	IgG1	IgG2A	AB_10673511	AB_2750739
N195A/16	QKI-5	IgG1	IgG2A	AB_10676099	AB_2750741

N196/16	PARIS/ZNF746	IgG1	IgG2A	AB_10675299	AB_2750742
N201/35	Iduna/RNF146	IgG1	IgG2A	AB_10675284	AB_2750744
N205B/22	LRRTM4	IgG1	IgG2A	AB_10674105	AB_2750745
N206A/8	GFAP	IgG1	IgG2A	AB_10672298	AB_2750746
N206B/9	GFAP R416WT	IgG1	IgG2A	AB_11000181	AB_2750747
N212/17	TRIP8b (constant)	IgG2a	IgG2A	AB_10675453	AB_2750748
N212/3	TRIP8b (exon 4)	IgG1	IgG2A	AB_2162409	AB_2750749
N212/7	TRIP8b (constant)	IgG2b	IgG2A	AB_10698034	AB_2750750
N222/6	Clcn4	IgG1	IgG2A	AB_11001829	AB_2750752
N229A/32	GABA(A)R, Alpha6	IgG1	IgG2A	AB_2336906	AB_2750753
N230/21	MMACHC	IgG1	IgG2A	AB_10673282	AB_2750754
N235/22	Pan-FHF-A	IgG2b	IgG2A	AB_10672416	AB_2750755
N244/5	SynCAM4	IgG1	IgG2A	AB_10673109	AB_2750758
N268/19	TRPML3/Mucolipin-3	IgG2a	IgG2A	AB_11000172	AB_2750759
N269/73	Synaptotagmin-10	IgG1	IgG2A	AB_10672424	AB_2750760
N271/44	ASIC1	IgG1	IgG2A	AB_11000719	AB_2750762
N277/7	Synaptotagmin-12	IgG1	IgG2A	AB_2315939	AB_2750763
N278/19	Synaptotagmin-3	IgG1	IgG2A	AB_11001828	AB_2750764
N279B/27	GluK5/Grik5/KA2 kainate receptor	IgG2a	IgG2A	AB_2315855	AB_2750765
N289/16	SUR1	IgG1	IgG2A	AB_11001671	AB_2750767
N291C/22	TRIP8b (exon 1a/5)	IgG1	IgG2A	AB_2315949	AB_2750769
N295B/54	Arl13b	IgG2b	IgG2A		AB_2750770
N295B/66	Arl13b	IgG2a	IgG2A	AB_11000053	AB_2750771
N320/48	Kirrel3, short isoform 3	IgG2a	IgG2A	AB_11030249	AB_2750773
N321C/49	Kirrel3, short and long	IgG2b	IgG2A	AB_2315856	AB_2750774
N323B/20	SUR2B	IgG2b	IgG2A	AB_2341102	AB_2750775
N325B/65	THAP1	IgG3	IgG2A	AB_2315943	AB_2750776
N326D/29	REEP1/2	IgG1	IgG2A	AB_2315914	AB_2750777
N328B/37	ZNF423	IgG1	IgG2A	AB_2315960	AB_2750778
N331/19	Dopamine D3 receptor	IgG2a	IgG2A	AB_2315831	AB_2750779
N341/37	LRRK1	IgG2a	IgG2A	AB_2315877	AB_2750781
N346/9	Stonin-2	IgG2b	IgG2A	AB_2315923	AB_2750782
N348/82	NSD3	IgG1	IgG2A	AB_2315901	AB_2750783
N353/13	Flrt3	IgG1	IgG2A	AB_2315832	AB_2750784
N355/1	GluA1/GluR1 glutamate receptor	IgG1	IgG2A	AB_2315839	AB_2750785
N356/23	SVOP	IgG1	IgG2A	AB_2315933	AB_2750786

N359/28	Foxi3	IgG1	IgG2A	AB_2315836	AB_2750787
N388A/10	Ankyrin-R	IgG2b	IgG2A	AB_2336901	AB_2750789
N388A/60	Pan-Ankyrin	IgG1	IgG2A	AB_2336913	AB_2750790
N398A/34	GABA(A)R, Alpha4	IgG1	IgG2A	AB_2336905	AB_2750791
N413/67	GABA(A)R, Epsilon	IgG2a	IgG2A	AB_2341105	AB_2750793
N415/24	GABA(A)R, Alpha5	IgG1	IgG2A	AB_2491075	AB_2750794
N419/40	Pan-Nav1 Na+ channel	IgG2a	IgG2A	AB_2491079	AB_2750795
N419/78	Pan-Nav1 Na+ channel	IgG1	IgG2A	AB_2491081	AB_2750796

820

821

822 **Table 4. Non-R-mAb antibodies used in this study**

823

Antibody	Immunogen	Manufacturer information	Concentration/ dilution used	Figures
KC	Synthetic peptide aa 837-853 of rat Kv2.1	Rabbit pAb, In-house (Trimmer Laboratory), RRID:AB_2315767	Affinity purified, 1:100	4
PSD-95	Fusion protein aa 77-299 of human PSD-95	Rabbit pAb, In-house (Trimmer Laboratory), RRID:AB_2750832	Affinity purified, 1:150	3
K28/43	Fusion protein aa 77-299 of human PSD-95	Mouse IgG2a mAb, NeuroMab RRID:AB_10698024	Tissue culture supernatant, 1:5	3
K28/86	Fusion protein aa 77-299 of human PSD-95	Mouse IgG1 mAb, NeuroMab RRID:AB_10698179	Tissue culture supernatant, 1:5	3
K57/1	Synthetic peptide aa 209-225 of human Kv4.2	Mouse IgG1 mAb, NeuroMab RRID:AB_10672254	Tissue culture supernatant, 1:5	4
K65/35	Fusion protein aa 1308-1381 of rat CASPR	Mouse IgG1 mAb, NeuroMab, RRID:AB_10671175	Tissue culture supernatant, 1:5	4
K89/34	Synthetic peptide aa 837-853 of rat Kv2.1	Mouse IgG1 mAb, NeuroMab catalog #73-014, RRID:AB_10672253	Tissue culture supernatant, 1:10	6
N28/9	Fusion protein aa 492-560 of rat VGluT1	Mouse IgG1 mAb, NeuroMab RRID:AB_10673111	Tissue culture supernatant, 1:5	4
N87/25	Fusion protein aa 370-433 of mouse GABA-A-receptor β3 subunit	Mouse IgG1 mAb, NeuroMab RRID:AB_10673389	Tissue culture supernatant, 1:5	4
N106/65	Full-length recombinant human Ankyrin-G	Mouse IgG2a mAb, NeuroMab RRID:AB_10673449	Tissue culture supernatant, 1:5	4
N147/6	Fusion protein aa 1-341 (full-length) of human QKI-5	Mouse IgG2b mAb, NeuroMab RRID:AB_10671658	Tissue culture supernatant, 1:5	4
N206A/8	Synthetic peptide aa 411-422 of human GFAP	Mouse IgG1 mAb, NeuroMab RRID:AB_10672298	Tissue culture supernatant, 1:5	4

824

825

826 **References**

827 1. Taussig MJ, Fonseca C & Trimmer JS (2018) Antibody validation: a view from the
828 mountains. N Biotechnol 45:1-8. DOI: 10.1016/j.nbt.2018.08.002.
829 2. Harlow E & Lane D (1988) Antibodies. A laboratory manual (Cold Spring Harbor
830 Laboratory, Cold Spring Harbor, N.Y.) pp 519-538.
831 3. Greenfield EA (2014) Antibodies. A laboratory manual, second edition (Cold Spring Harbor
832 Laboratory Press, Cold Spring Harbor, N.Y.).
833 4. Busby M, Xue C, Li C, Farjoun Y, Gienger E, Yofe I, Gladden A, Epstein CB, Cornett EM,
834 Rothbart SB, Nusbaum C & Goren A (2016) Systematic comparison of monoclonal versus
835 polyclonal antibodies for mapping histone modifications by ChIP-seq. Epigenetics &
836 chromatin 9:49. DOI: 10.1186/s13072-016-0100-6.
837 5. Bradbury A & Pluckthun A (2015) Reproducibility: Standardize antibodies used in
838 research. Nature 518:27-29. DOI: 10.1038/518027a.
839 6. Andreeff M, Bartal A, Feit C & Hirshaut Y (1985) Clonal stability and heterogeneity of
840 hybridomas: analysis by multiparameter flow cytometry. Hybridoma 4:277-287. DOI:
841 10.1089/hyb.1985.4.277.
842 7. Barnes LM, Bentley CM & Dickson AJ (2003) Stability of protein production from
843 recombinant mammalian cells. Biotechnol Bioeng 81:631-639. DOI: 10.1002/bit.10517.
844 8. Zack DJ, Wong AL, Stempniak M & Weisbart RH (1995) Two kappa immunoglobulin light
845 chains are secreted by an anti-DNA hybridoma: implications for isotypic exclusion. Mol
846 Immunol 32:1345-1353.
847 9. Blatt NB, Bill RM & Glick GD (1998) Characterization of a unique anti-DNA hybridoma.
848 Hybridoma 17:33-39. DOI: 10.1089/hyb.1998.17.33.
849 10. Bradbury ARM, Trinklein ND, Thie H, Wilkinson IC, Tandon AK, Anderson S, Bladen CL,
850 Jones B, Aldred SF, Bestagno M, Burrone O, Maynard J, Ferrara F, Trimmer JS,
851 Gornemann J, Glanville J, Wolf P, Frenzel A, Wong J, Koh XY, Eng HY, Lane D, Lefranc
852 MP, Clark M & Dubel S (2018) When monoclonal antibodies are not monospecific:
853 Hybridomas frequently express additional functional variable regions. MAbs 10:539-546.
854 DOI: 10.1080/19420862.2018.1445456.
855 11. Backliwal G, Hildinger M, Chenuet S, Wulhfard S, De Jesus M & Wurm FM (2008) Rational
856 vector design and multi-pathway modulation of HEK 293E cells yield recombinant antibody
857 titers exceeding 1 g/l by transient transfection under serum-free conditions. Nucleic Acids
858 Res 36:e96. DOI: 10.1093/nar/gkn423.
859 12. Fischer S, Handrick R & Otte K (2015) The art of CHO cell engineering: A comprehensive
860 retrospect and future perspectives. Biotechnol Adv 33:1878-1896. DOI:
861 10.1016/j.biotechadv.2015.10.015.
862 13. Kunert R & Reinhart D (2016) Advances in recombinant antibody manufacturing. Appl
863 Microbiol Biotechnol 100:3451-3461. DOI: 10.1007/s00253-016-7388-9.
864 14. Bekele-Arcuri Z, Matos MF, Manganas L, Strassle BW, Monaghan MM, Rhodes KJ &
865 Trimmer JS (1996) Generation and characterization of subtype-specific monoclonal
866 antibodies to K+ channel alpha- and beta-subunit polypeptides. Neuropharmacology
867 35:851-865.
868 15. Rhodes KJ, Strassle BW, Monaghan MM, Bekele-Arcuri Z, Matos MF & Trimmer JS
869 (1997) Association and colocalization of the Kvbeta1 and Kvbeta2 beta-subunits with Kv1
870 alpha-subunits in mammalian brain K+ channel complexes. J Neurosci 17:8246-8258.
871 16. Lim ST, Antonucci DE, Scannevin RH & Trimmer JS (2000) A novel targeting signal for
872 proximal clustering of the Kv2.1 K+ channel in hippocampal neurons. Neuron 25:385-397.
873 DOI: S0896-6273(00)80902-2 [pii].
874 17. Rasband MN, Park EW, Vanderah TW, Lai J, Porreca F & Trimmer JS (2001) Distinct
875 potassium channels on pain-sensing neurons. Proc Natl Acad Sci U S A 98:13373-13378.

18. Manning CF, Bundros AM & Trimmer JS (2012) Benefits and pitfalls of secondary antibodies: why choosing the right secondary is of primary importance. PLoS One 7:e38313. DOI: 10.1371/journal.pone.0038313.
19. Kennedy PJ, Oliveira C, Granja PL & Sarmento B (2018) Monoclonal antibodies: technologies for early discovery and engineering. Crit Rev Biotechnol 38:394-408. DOI: 10.1080/07388551.2017.1357002.
20. Wang X, Mathieu M & Brezski RJ (2018) IgG Fc engineering to modulate antibody effector functions. Protein Cell 9:63-73. DOI: 10.1007/s13238-017-0473-8.
21. Bradbury AR, Sidhu S, Dubel S & McCafferty J (2011) Beyond natural antibodies: the power of in vitro display technologies. Nat Biotechnol 29:245-254. DOI: 10.1038/nbt.1791.
22. Crosnier C, Staudt N & Wright GJ (2010) A rapid and scalable method for selecting recombinant mouse monoclonal antibodies. BMC Biol 8:76. DOI: 10.1186/1741-7007-8-76.
23. Rhodes KJ & Trimmer JS (2006) Antibodies as valuable neuroscience research tools versus reagents of mass distraction. J Neurosci 26:8017-8020. DOI: 26/31/8017 [pii] 10.1523/JNEUROSCI.2728-06.2006.
24. Gong B, Murray KD & Trimmer JS (2016) Developing high-quality mouse monoclonal antibodies for neuroscience research - approaches, perspectives and opportunities. N Biotechnol 33:551-564. DOI: 10.1016/j.nbt.2015.11.007.
25. Muller-Sienerth N, Crosnier C, Wright GJ & Staudt N (2014) Cloning of recombinant monoclonal antibodies from hybridomas in a single mammalian expression plasmid. Methods Mol Biol 1131:229-240. DOI: 10.1007/978-1-62703-992-5_14.
26. Durocher Y, Perret S & Kamen A (2002) High-level and high-throughput recombinant protein production by transient transfection of suspension-growing human 293-EBNA1 cells. Nucleic Acids Res 30:E9.
27. Rasband MN, Park EW, Zhen D, Arbuckle MI, Poliak S, Peles E, Grant SG & Trimmer JS (2002) Clustering of neuronal potassium channels is independent of their interaction with PSD-95. J Cell Biol 159:663-672.
28. Shibata R, Misonou H, Campomanes CR, Anderson AE, Schrader LA, Doliveira LC, Carroll KI, Sweatt JD, Rhodes KJ & Trimmer JS (2003) A fundamental role for KChIPs in determining the molecular properties and trafficking of Kv4.2 potassium channels. J Biol Chem 278:36445-36454.
29. Shi G, Kleinklaus AK, Marrion NV & Trimmer JS (1994) Properties of Kv2.1 K+ channels expressed in transfected mammalian cells. J Biol Chem 269:23204-23211.
30. Kim E, Niethammer M, Rothschild A, Jan YN & Sheng M (1995) Clustering of Shaker-type K+ channels by interaction with a family of membrane-associated guanylate kinases. Nature 378:85-88. DOI: 10.1038/378085a0.
31. Bishop HI, Guan D, Bocksteins E, Parajuli LK, Murray KD, Cobb MM, Misonou H, Zito K, Foehring RC & Trimmer JS (2015) Distinct cell- and layer-specific expression patterns and independent regulation of Kv2 channel subtypes in cortical pyramidal neurons. J Neurosci 35:14922-14942. DOI: 10.1523/JNEUROSCI.1897-15.2015.
32. Strassle BW, Menegola M, Rhodes KJ & Trimmer JS (2005) Light and electron microscopic analysis of KChIP and Kv4 localization in rat cerebellar granule cells. J Comp Neurol 484:144-155. DOI: 10.1002/cne.20443.
33. Krebber A, Bornhauser S, Burmester J, Honegger A, Willuda J, Bosshard HR & Pluckthun A (1997) Reliable cloning of functional antibody variable domains from hybridomas and spleen cell repertoires employing a reengineered phage display system. J Immunol Methods 201:35-55.
34. Haughton G, Lanier LL & Babcock GF (1978) The murine kappa light chain shift. Nature 275:154-157.

35. Woloschak GE & Krco CJ (1987) Regulation of kappa/lambda immunoglobulin light chain expression in normal murine lymphocytes. Mol Immunol 24:751-757.
36. Carroll WL, Mendel E & Levy S (1988) Hybridoma fusion cell lines contain an aberrant kappa transcript. Mol Immunol 25:991-995.
37. Shulman M, Wilde CD & Kohler G (1978) A better cell line for making hybridomas secreting specific antibodies. Nature 276:269-270.
38. Juste M, Muzard J & Billiald P (2006) Cloning of the antibody kappa light chain V-gene from murine hybridomas by bypassing the aberrant MOPC21-derived transcript. Anal Biochem 349:159-161. DOI: 10.1016/j.ab.2005.10.046.
39. Kistner U, Wenzel BM, Veh RW, Cases-Langhoff C, Garner AM, Appeltauer U, Voss B, Gundelfinger ED & Garner CC (1993) SAP90, a rat presynaptic protein related to the product of the Drosophila tumor suppressor gene dlg-A. J Biol Chem 268:4580-4583.
40. Rasband MN, Peles E, Trimmer JS, Levinson SR, Lux SE & Shrager P (1999) Dependence of nodal sodium channel clustering on paranodal axoglial contact in the developing CNS. J Neurosci 19:7516-7528.
41. Menegoz M, Gaspar P, Le Bert M, Galvez T, Burgaya F, Palfrey C, Ezan P, Arnos F & Girault JA (1997) Paranodin, a glycoprotein of neuronal paranodal membranes. Neuron 19:319-331.
42. Peles E, Nativ M, Lustig M, Grumet M, Schilling J, Martinez R, Plowman GD & Schlessinger J (1997) Identification of a novel contactin-associated transmembrane receptor with multiple domains implicated in protein-protein interactions. Embo j 16:978-988. DOI: 10.1093/emboj/16.5.978.
43. Zhang JH, Sato M & Tohyama M (1991) Region-specific expression of the mRNAs encoding beta subunits (beta 1, beta 2, and beta 3) of GABAA receptor in the rat brain. J Comp Neurol 303:637-657. DOI: 10.1002/cne.903030409.
44. Brenman JE, Topinka JR, Cooper EC, McGee AW, Rosen J, Milroy T, Ralston HJ & Bredt DS (1998) Localization of postsynaptic density-93 to dendritic microtubules and interaction with microtubule-associated protein 1A. J Neurosci 18:8805-8813.
45. Morrison SL & Scharff MD (1981) Mutational events in mouse myeloma cells. Crit Rev Immunol 3:1-22.
46. Frame KK & Hu WS (1990) The loss of antibody productivity in continuous culture of hybridoma cells. Biotechnol Bioeng 35:469-476. DOI: 10.1002/bit.260350504.
47. Castillo FJ, Mullen LJ, Grant BC, DeLeon J, Thrift JC, Chang LW, Irving JM & Burke DJ (1994) Hybridoma stability. Dev Biol Stand 83:55-64.
48. Drexler HG & Uphoff CC (2002) Mycoplasma contamination of cell cultures: Incidence, sources, effects, detection, elimination, prevention. Cytotechnology 39:75-90. DOI: 10.1023/A:1022913015916.
49. de Kovel CG, Brilstra EH, van Kempen MJ, Van't Slot R, Nijman IJ, Afawi Z, De Jonghe P, Djemie T, Guerrini R, Hardies K, Helbig I, Hendrickx R, Kanaan M, Kramer U, Lehesjoki AE, Lemke JR, Marini C, Mei D, Moller RS, Pendziwiat M, Stamberger H, Suls A, Weckhuysen S, Euro ERESC & Koeleman BP (2016) Targeted sequencing of 351 candidate genes for epileptic encephalopathy in a large cohort of patients. Mol Genet Genomic Med 4:568-580. DOI: 10.1002/mgg3.235.
50. Marini C, Romoli M, Parrini E, Costa C, Mei D, Mari F, Parmeggiani L, Procopio E, Metitieri T, Cellini E, Virdo S, De Vita D, Gentile M, Prontera P, Calabresi P & Guerrini R (2017) Clinical features and outcome of 6 new patients carrying de novo KCNB1 gene mutations. Neurol Genet 3:e206. DOI: 10.1212/NXG.0000000000000206.
51. Misonou H, Mohapatra DP, Park EW, Leung V, Zhen D, Misonou K, Anderson AE & Trimmer JS (2004) Regulation of ion channel localization and phosphorylation by neuronal activity. Nat Neurosci 7:711-718. DOI: 10.1038/nn1260nn1260 [pii].

52. Mandikian D, Bocksteins E, Parajuli LK, Bishop HI, Cerda O, Shigemoto R & Trimmer JS (2014) Cell type-specific spatial and functional coupling between mammalian brain Kv2.1 K(+) channels and ryanodine receptors. J Comp Neurol 522:3555-3574. DOI: 10.1002/cne.23641.
53. Trimmer JS (1991) Immunological identification and characterization of a delayed rectifier K+ channel polypeptide in rat brain. Proc Natl Acad Sci U S A 88:10764-10768.
54. Rhodes KJ, Keilbaugh SA, Barrezueta NX, Lopez KL & Trimmer JS (1995) Association and colocalization of K+ channel alpha- and beta-subunit polypeptides in rat brain. J Neurosci 15:5360-5371.
55. Knight KL, Burnett RC & McNicholas JM (1985) Organization and polymorphism of rabbit immunoglobulin heavy chain genes. J Immunol 134:1245-1250.
56. Stack EC, Wang C, Roman KA & Hoyt CC (2014) Multiplexed immunohistochemistry, imaging, and quantitation: a review, with an assessment of Tyramide signal amplification, multispectral imaging and multiplex analysis. Methods 70:46-58. DOI: 10.1016/j.ymeth.2014.08.016.
57. Natsuume-Sakai S, Motonishi K & Migita S (1977) Quantitative estimations of five classes of immunoglobulin in inbred mouse strains. Immunology 32:861-866.
58. Liu H, White J, Crawford F, Jin N, Ju X, Liu K, Jiang C, Marrack P, Zhang G & Kappler JW (2015) A rapid method to characterize mouse IgG antibodies and isolate native antigen binding IgG B cell hybridomas. PLoS One 10:e0136613. DOI: 10.1371/journal.pone.0136613.
59. Faguet GB & Agee JF (1993) A simple technique for the rapid enrichment of class and subclass hybridoma switch variants. A 1000-fold enrichment in half the time, for half the cost. J Immunol Methods 165:217-224.
60. Cochet O, Martin E, Fridman WH & Teillaud JL (1999) Selective PCR amplification of functional immunoglobulin light chain from hybridoma containing the aberrant MOPC 21-derived V kappa by PNA-mediated PCR clamping. Biotechniques 26:818-820, 822.
61. Duan L & Pomerantz RJ (1994) Elimination of endogenous aberrant kappa chain transcripts from sp2/0-derived hybridoma cells by specific ribozyme cleavage: utility in genetic therapy of HIV-1 infections. Nucleic Acids Res 22:5433-5438.
62. Yuan X, Gubbins MJ & Berry JD (2004) A simple and rapid protocol for the sequence determination of functional kappa light chain cDNAs from aberrant-chain-positive murine hybridomas. J Immunol Methods 294:199-207. DOI: 10.1016/j.jim.2004.09.001.
63. Ruberti F, Cattaneo A & Bradbury A (1994) The use of the RACE method to clone hybridoma cDNA when V region primers fail. J Immunol Methods 173:33-39.
64. Uhlen M, Bandrowski A, Carr S, Edwards A, Ellenberg J, Lundberg E, Rimm DL, Rodriguez H, Hiltke T, Snyder M & Yamamoto T (2016) A proposal for validation of antibodies. Nat Methods 13:823-827. DOI: 10.1038/nmeth.3995.
65. Ascoli CA & Aggeler B (2018) Overlooked benefits of using polyclonal antibodies. Biotechniques. DOI: 10.2144/btn-2018-0065.
66. Chen Y, Kim SH, Shang Y, Guillory J, Stinson J, Zhang Q, Hotzel I & Hoi KH (2018) Barcoded sequencing workflow for high throughput digitization of hybridoma antibody variable domain sequences. J Immunol Methods 455:88-94. DOI: 10.1016/j.jim.2018.01.004.

Figure legends

Figure 1. Schematic representation of the R-mAb pipeline. A. Schematic of cloning, expression and validation pipeline. Orange steps involve V_H and V_L regions of individual hybridomas, blue steps involve steps involving backbone components, and green step involves expression of target for R-mAb validation. B. Schematic shows the separate elements of the R-mAb expression plasmid involved in coexpression of light (green) and heavy (blue) chains as driven by two CMV promoters (orange). Hybridoma-derived V_L and V_H domain PCR products are fused to a joining fragment comprising a κ light chain constant domain (C_L) and the κ light chain polyA tail sequences (κ pA), a CMV promoter for heavy chain expression, and an ER signal/leader sequence (L) for translocation of the heavy chain across the ER membrane. PCR-mediated fusion of these three elements is followed by their insertion into the p1316 plasmid that contains an upstream CMV promoter for light chain expression, and an ER signal/leader sequence (L) for translocation of the light chain across the ER membrane. Downstream of the insert is a heavy chain constant domain (C_H) that is either γ1 or γ2a depending on the plasmid, followed by the SV40 polyA tail (SV40 pA).

Figure 2. Cloning of V_L and V_H domain sequences from hybridomas into the R-mAb expression plasmid. A. Agarose gel analysis of V_L and V_H domain PCR products amplified from cDNA synthesized from RNA extracted from the N59/36 (anti-NR2B/GRIN2B) and K39/25 (anti-Kv2.1/KCNB1) hybridomas. The expected size of mouse IgG V_L and V_H domains is ≈360 bp. B. Agarose gel analysis of V_H and digested V_L fragments joined by fusion PCR (F-PCR) to the P1316-derived joining fragment to create a dual IgG chain cassette. C. Agarose gel analysis of colony PCR samples of transformants from the N59/36 R-mAb project. D. Agarose gel analysis of products of restriction enzyme digestion of N59/36 plasmid DNA with NotI and AscI. The plasmid backbone is 7 kbp, and the intact insert comprising the V_L and V_H domains and the intervening joining fragment is 2.4 kbp. E. Agarose gel analysis of PCR products of V_L domain

cDNA synthesized from RNA extracted from mouse splenocytes, the fusion partner Sp2/0-Ag14, and various hybridomas after digestion with the BciVI restriction enzyme to cleave the Sp2/0-Ag14-derived aberrant light chain product. The intact V_L domains are ≈360 bp, and the digested aberrant light chains ≈180 bp.

Figure 3. Validation of subclass-switched anti-PSD-95 K28/43R R-mAb. A. Validation of the K28/43R R-mAb in heterologous cells. COS-1 cells transiently transfected to express human PSD-95 in a subset of cells were immunolabeled with K28/43 mAb (IgG2a) alone (top row), K28/43R R-mAb (IgG1) alone (middle row), or K28/43 mAb plus K28/43R R-mAb (bottom row). Immunolabeling in all samples was detected with a cocktail of anti-mouse IgG2a (red, for the K28/43 mAb) and anti-mouse IgG1 (green, for the K28/43R R-mAb) subclass-specific Alexa Fluor conjugated secondary antibodies. Labeling in blue is for the DNA-specific dye Hoechst 33258 and shows nuclei of both transfected and untransfected cells. Scale bar in the lower right merged panel = 30 μm and holds for all panels in A. B. Validation of the K28/43R R-mAb in brain sections. A brain section from an adult rat was immunolabeled with K28/43 mAb plus K28/43R R-mAb and immunolabeling detected with a cocktail of anti-mouse IgG2a (red, for K28/43 mAb) and anti-mouse IgG1 (green, for K28/43R R-mAb) subclass-specific Alexa Fluor conjugated secondary antibodies. Cell nuclei are labeled with the DNA-specific dye Hoechst 33258 (blue). The region of interest shown is from cerebellar cortex. Scale bar in the left panel = 100 μm, and in the right merged panel = 30 μm. C-E. Immunoblots against COS cell lysates over-expressing various members of the MAGUK superfamily of scaffolding proteins. To confirm expression of MAGUK proteins, immunoblots were probed with rabbit anti-PSD-95 (red). Primary antibodies were detected with the appropriate combinations of fluorescently labeled species-specific anti-rabbit and subclass-specific anti-mouse IgG secondary Abs. Control indicates COS cells transfected with an empty vector. C. K28/43R R-mAb (IgG2a, green). D. K28/43R R-mAb (IgG1, blue). E. the

K28/43 mAb (IgG2a, green). The blot in E was also probed with the K28/86 mAb (anti-pan-MAGUK, IgG1, blue).

Figure 4. Multiplex immunolabeling with subclass-switched recombinant antibodies in adult rat brain. A. Sections from neocortex labeled with anti-pan-Nav R-mAb K58/35R (IgG2a, red) at nodes of Ranvier and AIS, anti-CASPR mAb K65/35 (IgG1, green) at paranodes, and anti-Kv2.1 rabbit polyclonal (KC) antibody (blue) on somata and proximal dendrites. Scale bar = 150 μm. Insets (dashed box) show details of labeling for pan-Nav (red) and CASPR (green) at a single node of Ranvier as indicated by box in main panel. B. Sections through cerebellum show labeling with anti-GABA-AR β1 R-mAb N96/55R (IgG2a, magenta) in the molecular layer (ML), and anti-GABA-AR β3 mAb N87/25 (IgG1, green) in the granule cell layer (GL). PCL = Purkinje cell layer. Scale bar = 150 μm. C. Hippocampus sections labeled with anti-Kv2.1 R-mAb 89/34R (IgG2a, red) on somata and proximal dendrites, anti-AnkyrinG mAb N106/65 (IgG2b, green) on AIS, and nuclear stain Hoechst 33258 (blue). Scale bar = 150 μm. Panels C1-C3 show magnified details of labeling for pan-Kv2.1 (red) on somata and proximal dendrites, and anti-AnkyrinG (green) on AIS. Scale bar = 50 μm (C1-C3). D. Sections through cerebellum labelled with anti-GABA-AR α6 R-mAb K229A/32R (IgG2a, red) in the granule cell layer (GL), anti-pan-QKI mAb N147/6 (IgG2b, green) labeling glial cells in/near the Purkinje cell layer (PCL), and anti-Kv4.2 mAb K57/1 (IgG1, blue) labeling the granule cell layer (GL). Scale bar = 30 μm. E. Sections from neocortex labelled with anti-Kv2.1 R-mAb 89/34R (IgG2a, red) on somata and proximal dendrites of neurons, and anti-GFAP mAb N206A/8 (IgG1, green) and anti-pan-QKI mAb N147/6 (IgG2b, blue) labeling glial cell processes and cell bodies respectively. Scale bar = 15 μm. F. Sections through cerebellum show labeling with anti-PSD-93 R-mAb N18/30R (IgG2a, red) in the cell bodies and dendrites of Purkinje cells, the nuclear stain Hoechst 33258 (green) and anti-VGluT1 mAb N28/9 (IgG1, blue) in the molecular layer (ML). PCL = Purkinje cell layer. Scale bar = 10 μm.

Figure 5. Cloning of anti-Kv2.1 D3/71 V_L and V_H domain cDNAs from a nonviable hybridoma. A. Agarose gel analysis of PCR amplified V_L and V_H domains from cDNA synthesized from RNA extracted from the non-viable D3/71 hybridoma. The panel to the right shows the V_L after digestion with the BciVI restriction enzyme to cleave the Sp2/0-Ag14-derived aberrant light chain product. The expected size of mouse IgG V_L and V_H domains is ≈360 bp, and of the cleaved aberrant V_L domain is ≈180 bp. B. Agarose gel analysis of D3/71 V_H and digested V_L fragments joined by fusion PCR (F-PCR) to the P1316 joining fragment to create a dual IgG chain cassette. C. Agarose gel analysis of colony PCR samples of transformants from the of D3/71 R-mAb project. D. Agarose gel analysis of products of restriction enzyme digestion of D3/71 plasmid DNA with NotI and AscI. The plasmid backbone is 7 kbp, and the intact insert comprising the V_L and V_H domains and the intervening joining fragment is 2.4 kbp.

Figure 6. Recovery of a functional anti-Kv2.1 D3/71R R-mAb from nonviable hybridomas. A. Validation of the D3/71R R-mAb in heterologous cells. COS-1 cells transiently transfected to express rat Kv2.1 in a subset of cells were immunolabeled with K89/34 mAb (IgG1) alone (top row), D3/71R R-mAb (IgG2a) alone (middle row), or K89/34 mAb plus D3/71R R-mAb (bottom row). Immunolabeling in all samples was detected with a cocktail of anti-mouse IgG1 (green, for the K89/34 mAb) and anti-mouse IgG2a (red, for the D3/71R R-mAb) subclass-specific Alexa Fluor conjugated secondary antibodies. B. Validation of the subclass-switched K89/34R R-mAb in heterologous cells. COS-1 cells transiently transfected to express rat Kv2.1 in a subset of cells were immunolabeled with K89/34 mAb (IgG1) alone (top row), K89/34R R-mAb (IgG2a) alone (middle row), or K89/34 mAb plus K89/34R R-mAb (bottom row). Immunolabeling in all samples was detected with a cocktail of anti-mouse IgG1 (green, for the K89/34 mAb) and anti-mouse IgG2a (red, for the K89/34R R-mAb) subclass-specific Alexa Fluor conjugated secondary antibodies. Labeling in blue in panels A and B is for the DNA-specific dye Hoechst 33258 and shows nuclei of both transfected and untransfected cells. Scale bar in the lower right merged

panel = 30 µm and holds for all panels in A and B. C. Validation of the D3/71R R-mAb in brain sections. A brain section from an adult rat was immunolabeled with K89/34 mAb plus D3/71 R-mAb and the immunolabeling detected with a cocktail of anti-mouse IgG1 (green, for the K89/34 mAb) and anti-mouse IgG2a (red, for the D3/71R R-mAb) subclass-specific Alexa Fluor conjugated secondary antibodies. Cell nuclei are labeled with the DNA-specific dye Hoechst 33258 (blue). Region of interest shown is from neocortex. Scale bar = 30 µm. D. Strip immunoblots on a crude rat brain membrane fraction immunolabeled with the K89/34 mAb, the K89/34R R-mAb, and the D3/71 R-mAb as indicated. Immunolabeling was detected on autoradiography film after treatment of strip immunoblots with HRP-conjugated anti-mouse IgG-specific secondary antibody and ECL.

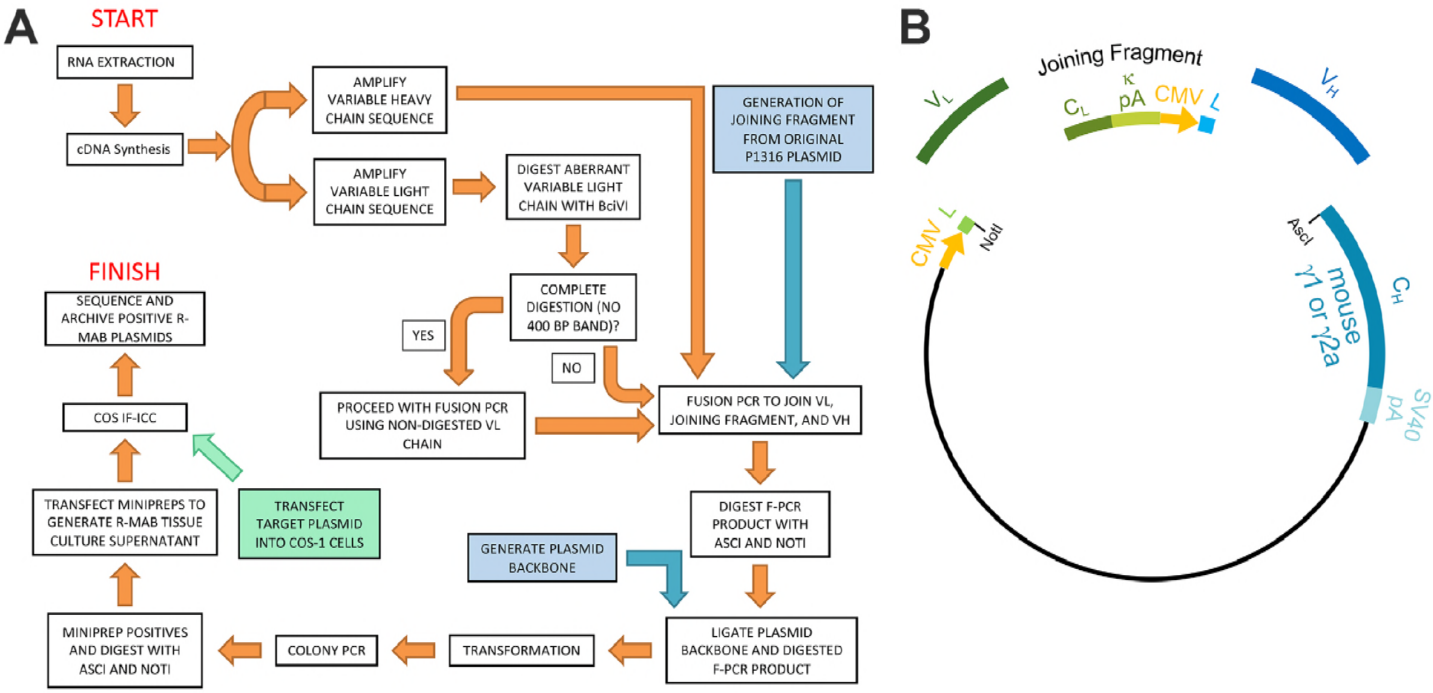

Figure 1

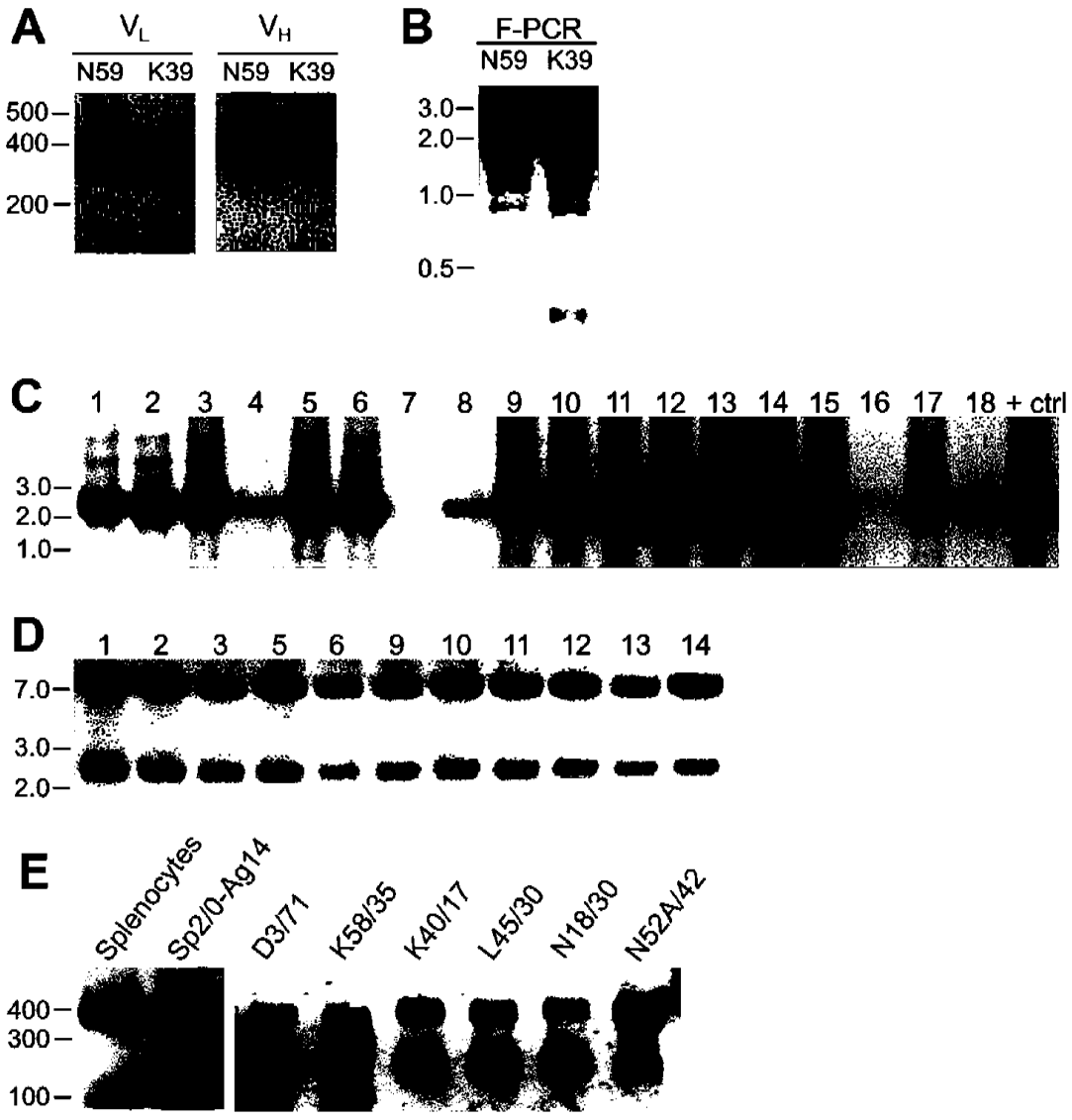

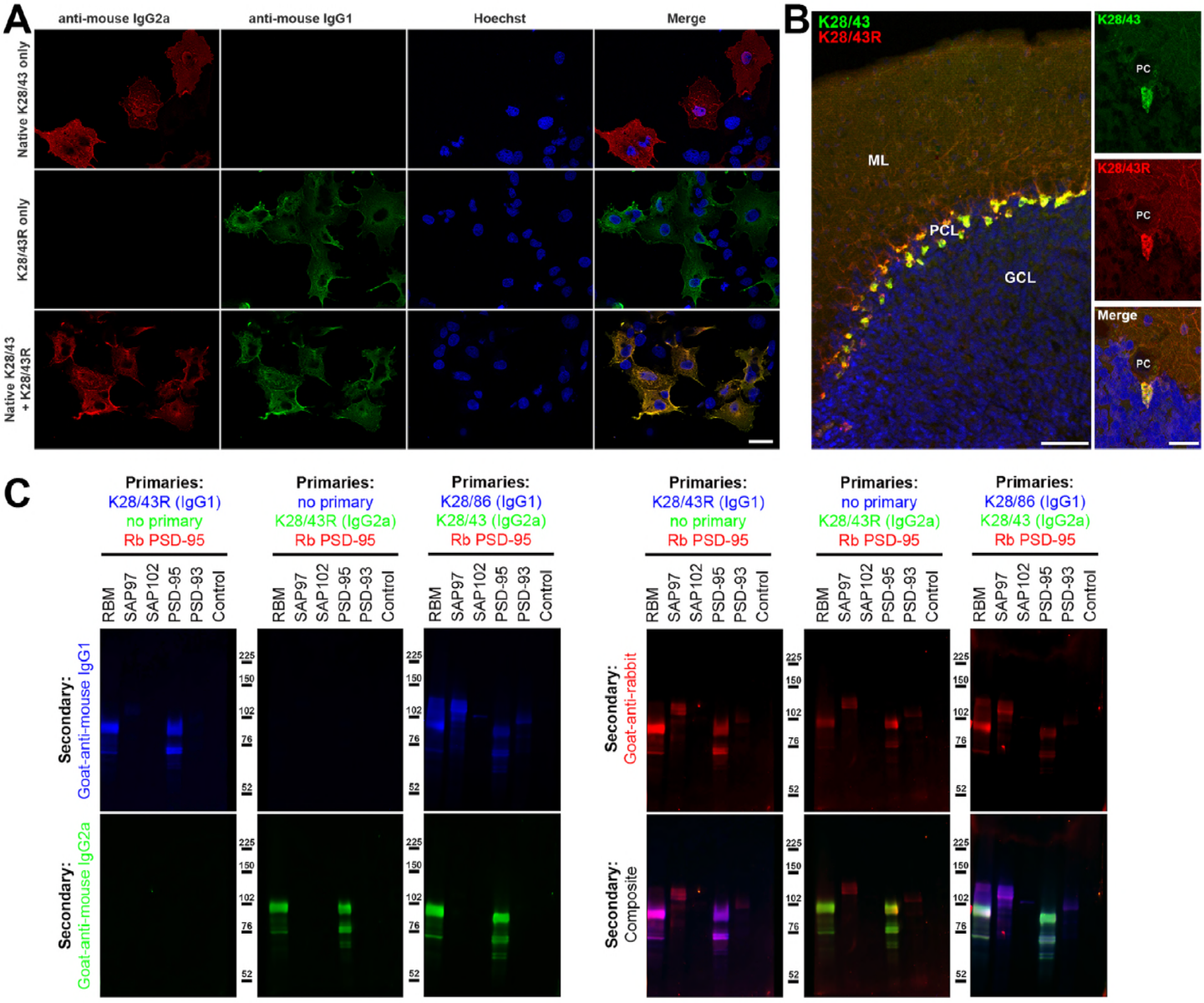

Figure 3

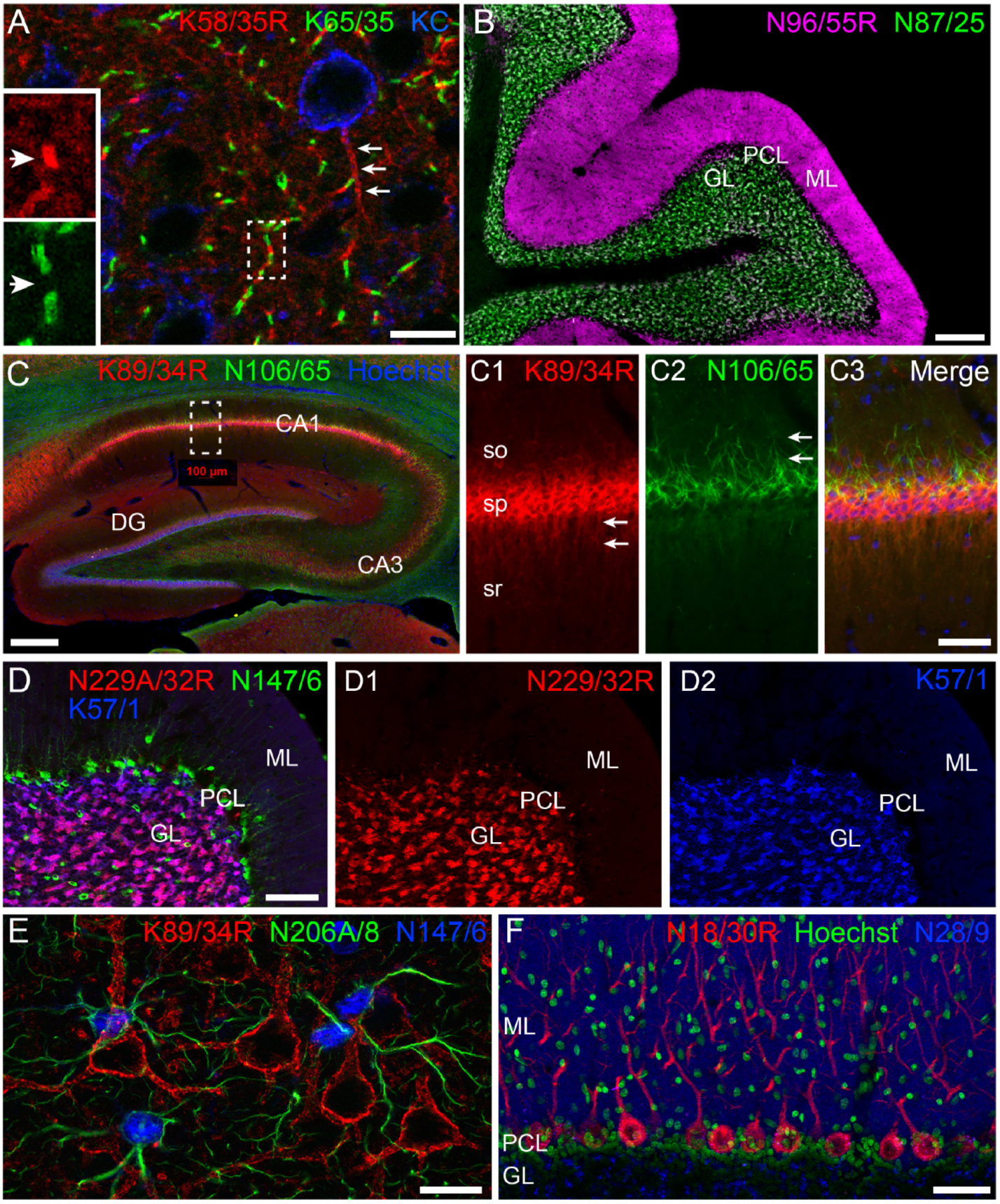

Figure 4

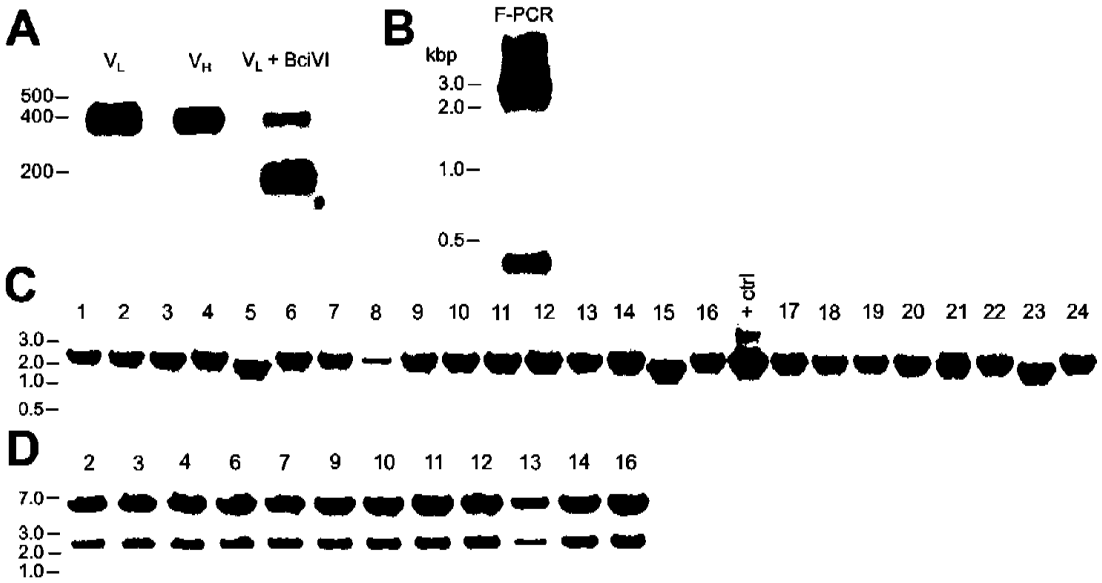

Figure 5

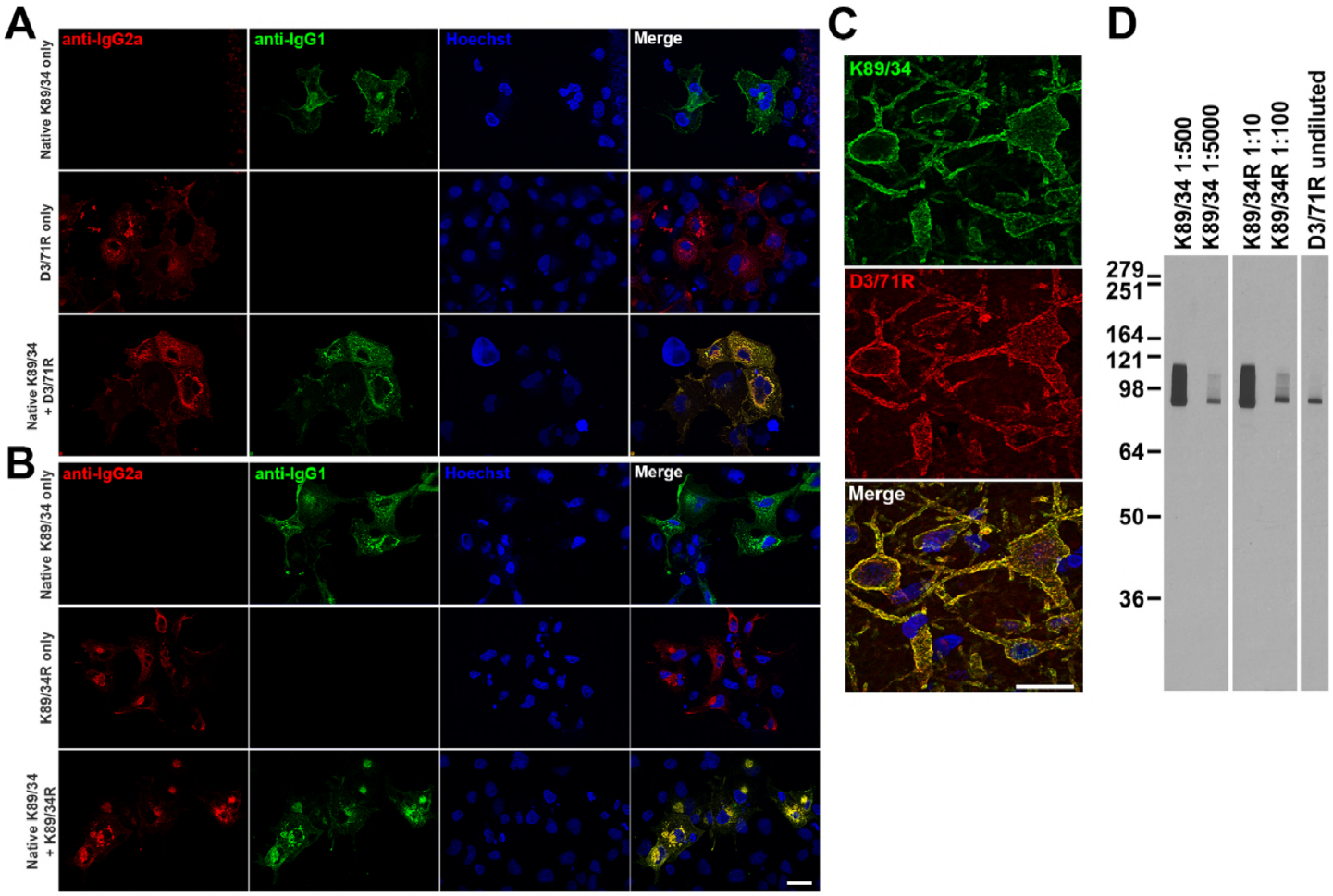

Figure 6